Combustion Science and Technology

ISSN: 0010-2202 (Print) 1563-521X (Online) Journal homepage: www.tandfonline.com/journals/gcst20

Evolution of Displacement Speed Statistics During Head-On Flame-Wall Interaction within Turbulent Boundary Layers

Gulcan Ozel-Erol, Umair Ahmed & Nilanjan Chakraborty

To cite this article: Gulcan Ozel-Erol, Umair Ahmed & Nilanjan Chakraborty (2024) Evolution of Displacement Speed Statistics During Head-On Flame-Wall Interaction within Turbulent Boundary Layers, Combustion Science and Technology, 196:13, 1990-2019, DOI: 10.1080/00102202.2024.2378491

To link to this article: https://doi.org/10.1080/00102202.2024.2378491

Published online: 24 Jul 2024.

Submit your article to this journal

Article views: 114

View related articles

View Crossmark data

Citing articles: 2 View citing articles

Full Terms & Conditions of access and use can be found at
https://www.tandfonline.com/action/journalInformation?journalCode=gcst20

COMBUSTION SCIENCE AND TECHNOLOGY
2024, VOL. 196, NO. 13, 1990–2019
https://doi.org/10.1080/00102202.2024.2378491

Taylor & Francis
Taylor & Francis Group

Check for updates

Evolution of Displacement Speed Statistics During Head-On Flame-Wall Interaction within Turbulent Boundary Layers

Gulcan Ozel-Erol[a], Umair Ahmed[b], and Nilanjan Chakraborty[b]

[a]Department of Mechanical Engineering, Bilecik Seyh Edebali University, Bilecik, Turkey; [b]School of Engineering, Newcastle University, Newcastle-Upon-Tyne, UK

ABSTRACT

The statistical behaviours of the density-weighted displacement speed and its curvature and strain rate dependence during head-on interaction of statistically planar premixed flames have been analysed based on Direct Numerical Simulations. The analysis has been conducted within turbulent boundary layers featuring inert walls, under both isothermal and adiabatic wall boundary conditions. The flame quenches due to heat loss when it reaches close to the wall in the case of isothermal wall boundary condition. By contrast, the flame can propagate all the way to the wall before extinguishing due to the consumption of reactants in the case of adiabatic wall boundary conditions. Thus, the effects of thermal expansion, quantified by dilatation rate, and flame normal acceleration during flame-wall interaction in the case of the isothermal wall are weaker than that in the case of the adiabatic wall case due to flame quenching. This gives rise to significant differences in the curvature and strain rate dependences of the reactive scalar gradient magnitude, which affects the statistical behaviours of the reaction and normal diffusion components of density-weighted displacement speed including their mean values, widths of their probability density functions, and their local strain rate and curvature dependences. It has been found that the interaction of near-wall vortical structures with flame surface increases the range of curvature variation during head-on interaction, which acts to widen the probability density function of the density-weighted displacement speed. This trend is relatively stronger for the isothermal wall boundary condition because of the larger variation of the reaction rate component of the density-weighted displacement speed due to local flame quenching, which also acts to widen the range of the density-weighted displacement speed variation in comparison to that in the case of adiabatic wall boundary conditions. Although the qualitative nature of curvature, strain rate, and stretch rate dependences of the density-weighted displacement speed remain unaffected by the wall boundary condition, the strength of the correlation changes with the progress of head-on interaction. It has been found that the negative correlation between the density-weighted displacement speed and flame curvature weakens with the progress of head-on interaction, which gives rise to a reduction in the strength of the correlation between the density-weighted displacement speed and flame stretch

ARTICLE HISTORY
Received 28 September 2023
Revised 11 December 2023
Accepted 19 January 2024

KEYWORDS
Density-weighted displacement speed; head-on flame-wall interaction; premixed flame; turbulent boundary layer; direct numerical simulations

CONTACT Gulcan Ozel-Erol gulcan.ozel@bilecik.edu.tr Department of Mechanical Engineering, Bilecik Seyh Edebali University, Bilecik 11100, Turkey

Published as part of the Special Issue based on work originally presented in 2023 at the 29th International Colloquium on the Dynamics of Explosions and Reactive Systems in Siheung, Korea the 29th International Colloquium on the Dynamics of Explosions and Reactive Systems in Beijing, China

© 2024 Taylor & Francis Group, LLC

rate. Similarly, the correlation between the tangential strain rate and the density-weighted displacement speed weakens with the progress of head-on interaction. Detailed physical explanations are provided for these behaviours, and their modeling implications are indicated.

Introduction

The speed with which a premixed flame surface propagates normally to itself with respect to an initially coincident material surface is known as the displacement speed S_d. Several previous studies (e.g., Echekki and Chen 1996, 1999; Peters et al. 1998; Chakraborty and Cant 2004, 2005, 2006; Chakraborty 2007; Chen and Im 1998, 2000; Han and Huh 2008; Chakraborty, Klein, and Cant 2011; Chakraborty et al. 2011; Nivarti and Cant 2019; Herbert et al. 2020; Ozel-Erol, Klein, and Chakraborty 2021; Keil et al. 2021a, 2021b; Chakraborty et al. 2022 and references therein) concentrated on the statistics of displacement speed S_d of turbulent premixed flames along with their strain rate and curvature dependencies because of their importance in level-set (Peters 2000) and Flame Surface Density (Chakraborty and Cant 2007, 2009; Hawkes and Cant 2001) based methodologies of turbulent premixed combustion modelling. The previous analyses (e.g., Gran, Echekki, and Chen 1996; Echekki and Chen 1996, 1999; Peters et al. 1998; Chakraborty and Cant 2004, 2005, 2006; Chakraborty 2007; Ozel-Erol, Klein, and Chakraborty 2021; Keil et al. 2021a, 2021b) revealed that the displacement speed shows mostly positive values within turbulent flames but a finite probability of negative values are obtained in the thin reaction zones regime (Peters 2000). Moreover, for premixed turbulent flames with a Lewis number close to unity, displacement speed, and curvature are found to be strongly negatively correlated, whereas a weak positive correlation is obtained between the displacement speed and tangential strain rate (Chakraborty and Cant 2004, 2006; Chakraborty 2007; Keil et al. 2021a,2021b). These correlations are affected by Lewis number (e.g., Chakraborty and Cant 2005, 2006; Han and Huh 2008; Ozel-Erol, Klein, and Chakraborty 2021) with the correlations weakening with increasing turbulence intensity (Chakraborty, Klein, and Cant 2011, 2022; Herbert et al. 2020; Nivarti and Cant 2019). The tangential strain rate and curvature dependences of displacement speed are found to be non-linear, and this behaviour arises principally due to the correlations of reactive scalar gradient and chemical reaction rate with strain rate and curvature (Chakraborty and Cant 2004, 2005, 2006; Chakraborty 2007; Chakraborty, Klein, and Cant 2011; Ozel-Erol, Klein, and Chakraborty 2021; Keil et al. 2021a, 2021b), which in turn affect the reaction and normal diffusion components of displacement speed. Moreover, strain rate and curvature correlations with displacement speed give rise to a highly non-linear stretch rate dependence of displacement speed (Chakraborty et al. 2022; Chen and Im 1998, 2000; Herbert et al. 2020). All of these findings have been obtained for combustion processes occurring without the influence of boundary layers and flame-wall interaction (FWI).

Modern combustors are made smaller in size to increase power density and also to make them compatible with electrical powertrains, and thus FWI occurs more readily in these small-sized combustors than in conventional combustors. The statistical behaviour of the flame displacement speed S_d is determined by the imbalance between the chemical

reaction rate and molecular diffusion rate, and also by the reactive scalar gradient magnitude (Echekki and Chen 1996, 1999; Peters et al. 1998; Chakraborty and Cant 2004, 2005, 2006; Chakraborty 2007; Chakraborty, Klein, and Cant 2007, 2011b; Han and Huh 2008; Nivarti and Cant 2019; Ozel-Erol, Klein, and Chakraborty 2021; Keil et al. 2021a, 2021b). It has been demonstrated by Ahmed, Chakraborty, and Klein (2021c, 2021b) that the molecular diffusion rate and reactive scalar gradient are affected by the shear rate induced by the wall and the thermal boundary condition prevailing there. Therefore, a thorough understanding of displacement speed statistics is essential for the purpose of extending the existing modelling methodologies to address FWI accurately in Reynolds Averaged Navier-Stokes (RANS)/Large Eddy Simulations (LES) approaches. However, displacement statistics are rarely addressed in the case of FWI and recent analyses by Ahmed et al (2020, 2021a) reported the mean behaviours of displacement speed and its components in oblique FWI of a V-shaped flame and flashback in turbulent channel flows. The flame normal in a mean sense is at an angle with the wall-normal direction in the configuration analyzed by Ahmed et al (2020, 2021a), whereas displacement speed statistics are yet to be analysed in turbulent boundary layers for the head-on interaction (HOI) configuration, which is an unsteady configuration where the flame and wall-normal vectors are aligned with each other. The relative alignment of the flame normal vector with the wall normal vector can significantly alter the strain rate effects experienced by the flame (Ahmed, Chakraborty, and Klein 2023). Thus, the strain rate (and therefore stretch rate) effects experienced by the flame in the head-on interaction configuration are expected to be different from the oblique flame-wall interaction analysed by Ahmed, Chakraborty, and Klein (2021c). Note that only the mean behaviours of displacement speed and its components were reported by Ahmed, Chakraborty, and Klein (2021c), and the wall effects on local strain rate and curvature dependences of displacement speed at different stages of FWI during HOI within turbulent boundary layers are yet to be reported in the existing literature. It is expected that the mean behaviour of displacement speed and its local strain rate and curvature dependence are affected by the presence of the wall during HOI. The curvature and strain rate dependencies of displacement speed during FWI are essential for extending the FSD and level-set methodologies for FWI. However, the effects of wall boundary conditions on flame displacement speed statistics are yet to be analysed in detail.

In an attempt to fill the aforementioned gaps in the existing literature, the displacement speed statistics during FWI will be addressed in this analysis by using a three-dimensional Direct Numerical Simulations (DNS) database of HOI of statistically planar flames propagating across turbulent boundary layers (Ahmed, Chakraborty, and Klein 2021b, 2023; Ghai et al. 2022). Two different wall boundary conditions, namely, isothermal, and adiabatic walls, have been considered in this analysis to investigate the influence of wall boundary conditions on displacement speed statistics at different stages of FWI. It is worth noting that isothermal and adiabatic wall conditions are among the most commonly used boundary conditions in FWI analyses (Ahmed, Chakraborty, and Klein 2021b, 2023; Ghai et al. 2022). Isothermal and adiabatic boundary conditions are extreme limiting situations and the thermal wall boundary condition for combustor walls in engineering applications remains somewhere between these two limiting conditions. Thus, a comparison between isothermal and adiabatic walls helps to distinguish and understand the effects of heat transfer through the wall boundary on the flame propagation statistics during HOI of premixed flames

within turbulent boundary layers. A similar approach was adopted in several previous analyses (Ahmed, Chakraborty, and Klein 2021b, 2023; Ghai et al. 2022) to analyse different aspects of flame-wall interaction.

Note that HOI across a turbulent boundary layer is an unsteady event and thus the displacement speed statistics will be presented at time instants when the flame is at different distances from the wall and therefore at different stages of FWI. Thus, the main objectives of the present analysis are:

(a) to analyse the statistical behaviour of displacement speed and its curvature and strain rate dependences at different stages of FWI,
(b) to demonstrate and explain the influence of wall boundary conditions on the aspects described in (a).

The rest of the paper is organised in the following manner. The mathematical background and numerical implementation pertaining to this analysis are presented in the next two sections of this paper. Section 4 deals with the discussion of the results and in the last section the main findings are summarised, and conclusions are drawn.

Mathematical background

In premixed flames, a reaction progress variable c can be defined based on a suitable major species mass fraction Y as: $c = (Y_0 - Y)/(Y_0 - Y_\infty)$ with subscripts 0 and ∞ referring to values in unburned gas and fully burned products, respectively. The reaction progress variable is defined based on the fuel mass fraction in the current analysis. The transport equation of c takes the following form:

$$\rho\left(\partial c/\partial t + u_j \partial c/\partial x_j\right) = \dot{w} + \nabla \cdot (\rho D \nabla c) \tag{1}$$

Here, ρ, u_j, D, and $\dot{w}$ are gas density, the j^{th} component of fluid velocity, progress variable diffusivity, and reaction rate of the progress variable, respectively. Equation 1 can be written in the kinematic form for a given c-isosurface in the following manner:

$$\left[\partial c/\partial t + u_j \partial c/\partial x_j\right] = S_d |\nabla c| \tag{2}$$

where S_d is the displacement speed, which can be expressed in the following manner (Echekki and Chen 1996, 1999; Peters et al. 1998):

$$S_d = [\dot{w} + \nabla \cdot (\rho D \nabla c)]/\rho |\nabla c| = S_r + S_n + S_t \tag{3}$$

Here, S_r, S_n, and S_t are the reaction, normal diffusion, and tangential diffusion components of displacement speed, which are given as (Echekki and Chen 1999; Peters et al. 1998):

$$S_r = \dot{w}/\rho |\nabla c|; S_n = \vec{N} \cdot \nabla \cdot \left(\rho D \vec{N} \cdot \nabla c\right)/\rho |\nabla c| \text{and} S_t = -2 D \kappa_m \tag{4}$$

where $\vec{N} = -\ c/|\ c|$ is the flame normal vector and $\kappa_m = 0.5\ \ \cdot \vec{N}$ is the local flame curvature. According to the current convention, the flame normal vector points towards the reactants and the flame surface convex (concave) towards the reactants has a positive (negative) curvature. In this respect, it is worthwhile to define the tangential strain rate a_T acting on a given c-isosurface as (Poinsot and Veynante, 2005):

$$a_T = \left(\delta_{ij} - N_i N_j\right)\partial u_i/\partial x_j \tag{5}$$

Here, u_i is the i^{th} component of fluid velocity. Both a_T and κ_m determine the stretch rate K affecting the flame surface (Chen and Im 1998, 2000; Poinsot and Veynante, 2005):

$$K = a_T + 2S_d\kappa_m \tag{6}$$

It can be seen from Equations 3 and 4 that the gas density ρ affects the displacement speed and its components, and thus, it is worthwhile to consider the density-weighted displacement speed $S_d^* = \rho S_d/\rho_0$ and its components: $S_r^* = \rho S_r/\rho_0$, $S_n^* = \rho S_n/\rho_0$, and $S_t^* = \rho S_t/\rho_0$ where ρ_0 is the unburned gas density. Moreover, S_d^* plays a key role in terms of modelling turbulent premixed combustion (Chakraborty and Cant 2007, 2009; Peters 2000). Thus, the statistics of S_d^* and its strain rate, curvature, and stretch rate dependences will be presented in Section 4 at different stages of HOI of statistically planar flames across turbulent boundary layers using DNS data.

Numerical implementation

The simulations used for this analysis have been carried out using a well-known code called SENGA+ (Jenkins and Cant 1999), which employs a 10^{th}-order central-difference scheme for approximating the spatial gradients for the internal grid points, but the order of accuracy gradually reduces to a one-sided second order scheme for the non-periodic boundaries. The time advancement is accounted for by a low storage third-order Runge-Kutta scheme (Wray 1990). A single-step irreversible Arrhenius-type chemical reaction for stoichiometric methane-air combustion (unit mass of Fuel + s unit mass of Oxidiser ➔ (1 +s) unit mass of Products, where $s = 4.0$ is the stoichiometric oxidiser-fuel mass ratio for methane-air mixture) is considered for the current analysis. The unburned gas temperature T_0 is considered to be 730 K (because unburned gas is often preheated in spark ignition engines and gas turbines). This yields a heat release rate parameter of $\tau = (T_{ad} - T_0)/T_0 = 2.3$, which is consistent with previous DNS analyses of FWI (Alshaalan and Rutland 1998, 2002; Gruber et al. 2010, 2012; Kitano et al. 2015). The Lewis number of all the species is taken to be unity for the sake of simplicity, and standard values are considered for the Prandtl number Pr and the ratio of specific heat, γ (i.e., $Pr = 0.7, \gamma = 1.4$).

Several previous studies demonstrated that the statistics of reactive scalar gradient (Chakraborty and Klein 2008; Chakraborty et al. 2008; Lai and Chakraborty 2016; Lai, Klein, and Chakraborty 2018), displacement speed (Peters et al. 1998; Echekki and Chen 1999; Keil et al. 2021a, 2021b; Chakraborty and Cant 2004; Chakraborty 2007), maximum wall heat flux magnitude (Lai and Chakraborty 2016; Lai et al. 2022; Lai, Klein, and Chakraborty 2018), and the flame quenching distance (Lai and Chakraborty 2016; Lai et al. 2022; Lai, Klein, and Chakraborty 2018) from simple chemistry are in good agreement with the corresponding results obtained from detailed chemistry. Moreover, a number of previous studies utilised single-step chemistry for head-on quenching simulations of premixed turbulent flames under initially isotropic turbulence conditions (Poinsot et al 1993; Ahmed et al. 2018; Lai and Chakraborty 2016; Sellmann et al. 2017), head-on quenching in a turbulent channel flow (Bruneaux et al. 1996), and also in a V-flame configuration (Alshaalan and Rutland 1998, 2002). It has been found that the inclusion of a detailed

chemical mechanism with variable transport properties does not affect flame dynamics (Lai et al. 2022; Lai, Klein, and Chakraborty 2018) or the behaviour of flame-turbulence interaction in the presence of inert isothermal walls (Ahmed et al. 2018). The previously proposed closures for the Flame Surface Density (FSD) and scalar dissipation rate (SDR) based on simple chemistry DNS data are found to be valid for detailed chemistry DNS data in the case of FWI (Lai et al. 2022; Lai, Klein, and Chakraborty 2018), and wall heat flux and wall Peclet number obtained from simple chemistry DNS are found to be in good agreement with experimental findings (Huang, Vosen, and Greif 1988; Jarosinski 1986; Vosen, Greif, and Westbrook 1985). The fluid-dynamical aspects of oblique-wall quenching of turbulent V-shaped premixed flames based on simple chemistry DNS data (Alshaalan and Rutland 1998, 2002) are consistent with detailed chemistry results (Gruber et al. 2010).

Recent analyses by Keil et al. (2021a, 2021b) revealed that the flame displacement speed statistics and its curvature and strain rate dependence obtained from single-step chemistry DNS data are found to be qualitatively similar to those obtained from the corresponding detailed chemistry DNS data. The quantitative differences in displacement statistics between single-step and detailed chemistry DNS are comparable to the uncertainties associated with different choices of reaction progress variables. Based on the body of aforementioned evidence, it can reasonably be expected that the simplification of chemistry is unlikely to affect the qualitative nature of the conclusions of this analysis.

The configuration, which has been employed for this analysis, considers a turbulent boundary layer on top of a chemically inert wall, and the initial flow condition is specified using a non-reacting fully developed turbulent channel flow solution corresponding to $Re_\tau = \rho_0 u_{\tau,NR} h/\mu_0 = 110$ where μ_0 is the unburned gas viscosity and h is the channel half height. It was recently reported that qualitative behaviour of mean values of displacement speed and its components during FWI within turbulent boundary layers does not change due to the variation of Re_τ (Kai et al. 2022).

The schematic diagram of the configuration is shown in Figure 1. The simulation domain size of $10.69h \times 1.33h \times 4h$ is discretised by an equidistant grid $1920 \times 240 \times 720$, which ensures at least 8 grid points within the thermal flame thickness $\delta_{th} = (T_{ad} - T_0)/\max|\ T|_L$ for $S_L/u_{\tau,NR} = 0.7$ with S_L, $u_{\tau,NR} = \sqrt{|\tau_{w.NR}|/\rho}$ and $\tau_{w,NR}$ are the unstretched laminar burning velocity, friction velocity, and wall shear stress for the non-reacting channel flow, respectively. The longitudinal integral length scale L_{11} and root-mean-square turbulent velocity u' remain of the order of h and $u_{\tau,NR}$, respectively, for

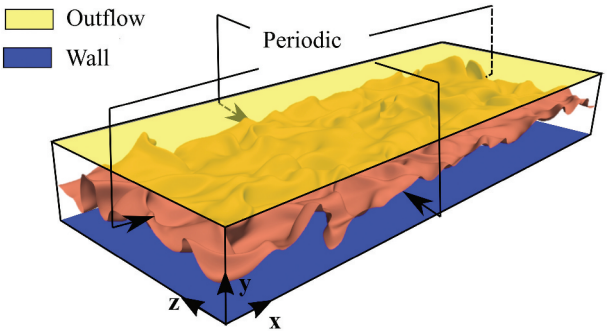

Figure 1. Schematic diagram of the simulation configuration.

the channel flow with $Re_\tau = 110$ (Ahmed et al. 2021). This leads to a Damköhler number $Da = L_{11}S_L/u'\delta_{th}$ of 15.80 and a Karlovitz number $Ka = (u'/S_L)^{3/2}(L_{11}/\delta_{th})^{-1/2}$ of 0.36 away from the wall, which suggests that the flame is expected to show the attributes of the corrugated flamelets regime combustion (Peters 2000) at early times. For these simulations, periodic boundary conditions are imposed for the streamwise (i.e., $x-$direction) and spanwise (i.e., $z-$direction) directions and the mean pressure gradient (i.e., $-\partial p/\partial x = \rho u^2_{\tau,NR}/h$ where p is the pressure) is imposed in the streamwise flow direction. Further information can be found in Ahmed, Chakraborty, and Klein (2021b, 2021c) regarding the validation of the non-reacting channel flow simulation, which is not repeated here for the sake of brevity. In the wall-normal direction (i.e., y-direction), a no-slip boundary condition is implemented at $y = 0$, and the temperature is imposed (i.e., $T_w = T_0$) for isothermal wall boundary conditions. For the adiabatic wall boundary condition, a Neumann boundary condition, given by $\partial T/\partial y = 0$ is specified at the wall. At $y/h = 1.33$, the boundary is taken to be partially non-reflecting. The wave amplitude variation L_1 for the acoustic wave that enters into the computational domain through the outflow boundary is specified as $L_1 = K(p - p_\infty)$ where p is the pressure, p_∞ is the intended mean thermodynamic pressure, and K is a constant which is defined as $K = \sigma\left(1 - Ma^2_{max}\right)a/L_{domain}$ (Haworth and Poinsot 1992) with a, L_{domain}, Ma_{max}, and σ being the acoustic speed, simulation domain length in the direction of the outflow boundary, the maximum Mach number in the flow, and a relaxation parameter, respectively. Setting the relaxation parameter σ to zero leads to a perfectly non-reflecting condition but this leads to mean pressure drift (Poinsot and Lele, 1992). On the other side, a large value of σ allows strong reflections from the outlet boundary. In the current analysis, the relaxation parameter σ is chosen to be 0.25 following the recommendation by Poinsot and Lele (1992), which offers a compromise between artificial wave reflection from the boundary and maintaining the desired mean pressure in the form of a partially non-reflecting boundary.

A steady freely propagating 1D laminar flame simulation is interpolated to the 3D grid in such a manner that $c = 0.5$ is obtained at $y/h \approx 0.85$ so that the reactant side of the flame faces the wall, and the product side of the flame faces towards the outflow side of the boundary in the $y-$direction. The simulations have been continued for 2.0 flow-through times which amounts to $21.30t_f$ where $t_f = \delta_{th}/S_L$ is the chemical timescale. The flames interact with the wall within this simulation duration, but the turbulent boundary layer does not evolve significantly during the simulation (Ahmed, Chakraborty, and Klein 2021b, 2021c; Ghai et al. 2022).

Results and discussion

Global features of head-on interaction (HOI)

The instantaneous views of the $\theta = (T - T_0)/(T_{ad} - T_0) = 0.8$ isosurfaces at different time instants are shown in Figure 2 for HOI within turbulent boundary layer for both isothermal and adiabatic wall boundary conditions. The time instants shown in Figure 2 are representative of the situations (i) when the flame is away from the wall (e.g., $t/t_f = 3.99$), (ii) it starts to interact with the wall (e.g., $t/t_f = 10.92$) and (iii) it is at the advanced stage of flame quenching (e.g., $t/t_f = 14.70$). The displacement speed

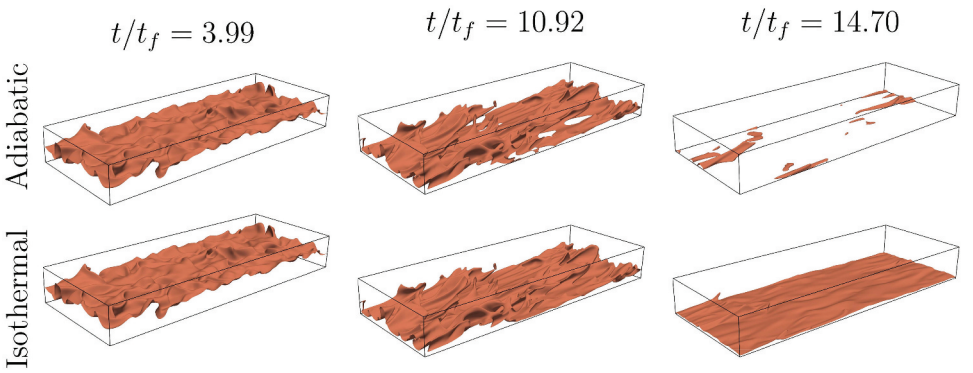

Figure 2. Temporal evolution of nondimensional temperature $\theta = 0.8$ isosurface for adiabatic (top) and isothermal (bottom) walls. The time instants correspond to $t/t_f = 3.99$, 10.92, and 14.70 (left to right).

statistics for the time instants when the flame is away from the wall (e.g., $t/t_f = 3.99$) are qualitatively similar to the findings from previous analyses without walls so a comparison of displacement speed statistics at different time instants in the HOI configuration provides insights into the wall effects on displacement speed statistics during FWI.

The choices of $\theta = 0.8$ and $c = 0.8$ are driven by the fact that the maximum chemical reaction for the freely propagating laminar premixed flame is obtained for approximately these values of θ and c for the current thermochemistry and thus the $c = 0.8$ isosurface will henceforth be considered as the flame surface in this paper. In the case of the adiabatic wall boundary condition, the flame does not quench but eventually extinguishes due to the consumption of reactants when it reaches the wall, which can be seen from the increasingly disappearing $\theta = 0.8$ isosurface in Figure 2 for this boundary condition. By contrast, in the case of the isothermal boundary condition the flame quenches due to heat loss at the wall when it reaches close to the wall and the unburned reactants from the vicinity of the wall diffuse to the regions away from the wall, whereas the burned products away from the wall diffuse towards the wall. Thus, a continuous $\theta = 0.8$ isosurface is obtained due to the thermal boundary layer on the isothermal wall. As a consequence of diffusion of burned (unburned) gas towards (away from) the wall, the value of c increases at the wall (i.e., $y = 0$) with the progress of HOI for the isothermal wall boundary condition and this trend is particularly visible at the advanced stages of HOI (e.g., $t/t_f = 14.70$). The chemical reaction can progress at the wall in the case of adiabatic boundary condition and the eventual consumption of the reactants at the wall in this case also increases c at the wall (i.e., $y = 0$) with the progress of HOI. The differences in near-wall behaviour of $\dot{w}$ between isothermal and adiabatic wall boundary conditions are reflected in the statistics of S_d^* and its components, which will be discussed next.

Statistical behaviour of reaction-diffusion imbalance

It can be appreciated from Equations 3 and 4 that the statistical behaviours of $\dot{w}$, $\quad\cdot(\rho D \quad c)$ and $|\quad c|$ affect the statistics of S_d^*. The variations of the mean values of $\dot{w}$, $\quad\cdot(\rho D \quad c)$, $\vec{N}\cdot\quad\left(\rho D\vec{N}\cdot\quad c\right)$, and $-2\rho D\kappa_m|\quad c|$ conditional upon c for different time instants are shown

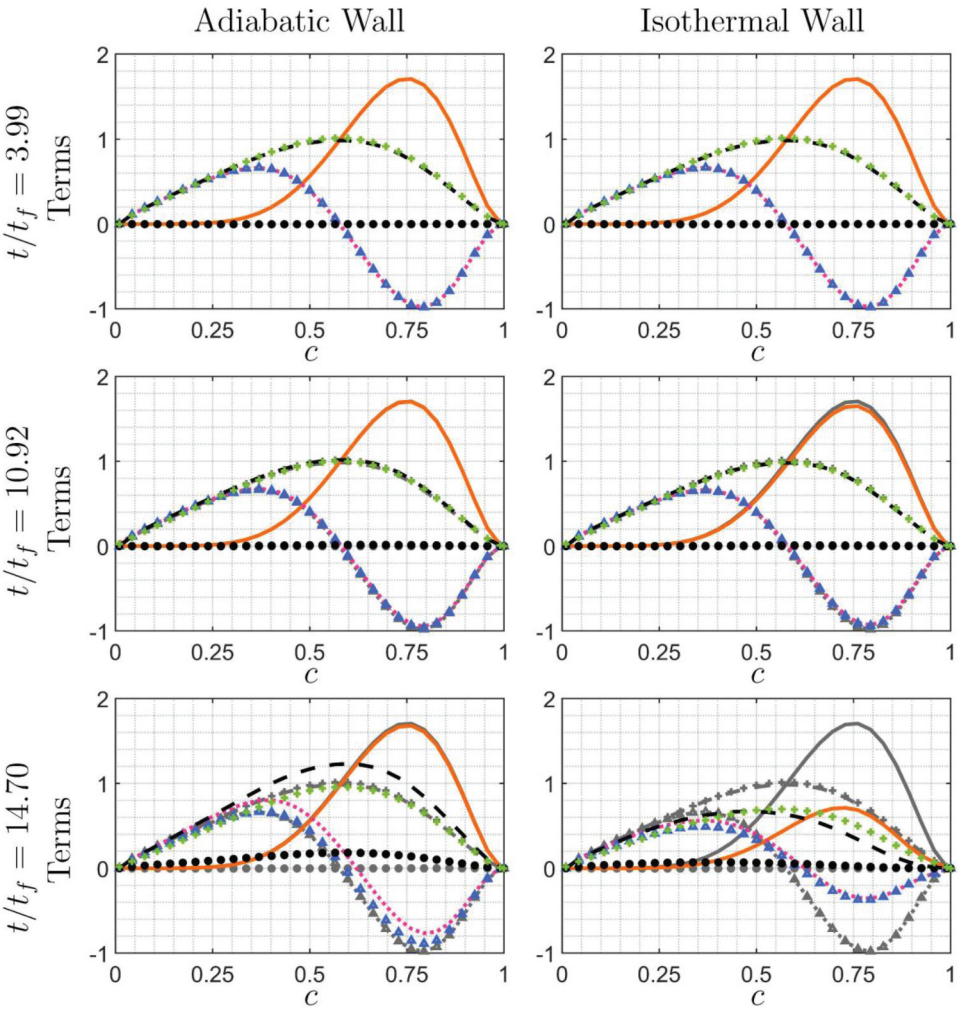

Figure 3. Variations of the mean values of {$\dot{w}$ (), $\cdot(\rho D\ c)$ (), $\vec{N}\cdot\left(\rho D\vec{N}\cdot\ c\right)$ (), $-2\rho D\kappa_m|\ c|$ (), $\dot{w}+\ \cdot(\rho D\ c)$ (), $\rho_0 S_L|\ c|$ (+ +) } $\times\ \delta_{th}/\rho_0 S_L$ conditional upon c at $t/t_f = 3.99$ (top), 10.92 (middle), and 14.70 (bottom) for adiabatic and isothermal walls. The corresponding quantities for unstretched laminar flames are shown by gray color and corresponding style.

in Figure 3 for both isothermal and adiabatic boundary conditions. The corresponding variations in the unstretched laminar premixed flame are also shown in Figure 3. It can be seen from Figure 3 that the variations of mean values of $\dot{w}$, $\cdot(\rho D\ c)$, $\vec{N}\cdot\ \left(\rho D\vec{N}\cdot\ c\right)$, and $-2\rho D\kappa_m|\ c|$ conditional upon c for isothermal and adiabatic boundary conditions remain identical to each other and almost equal to the corresponding variations in the unstretched laminar premixed flame when the flame remains away from the wall (e.g., $t/t_f = 3.99$). Figure 3 shows that the mean value of $\dot{w}$ assumes negligible values towards the unburned gas side but assumes the maximum value close to $c = 0.8$. The mean values of $\cdot(\rho D\ c)$ and $\vec{N}\cdot\ \left(\rho D\vec{N}\cdot\ c\right)$ assume positive values towards the unburned gas side of the flame front but they become negative on the burned gas side. Moreover, the mean values

of $\nabla\cdot(\rho D\nabla c) = \vec{N}\cdot\left(\rho D\vec{N}\cdot\nabla c\right) - 2\rho D\kappa_m|\nabla c|$ and $\vec{N}\cdot\left(\rho D\vec{N}\cdot\nabla c\right)$ are found to be almost equal to each other for the time instants when the flames are away from the wall (e.g., $t/t_f = 3.99$), which suggests that the mean contribution of $-2\rho D\kappa_m|\nabla c|$ is negligible. This behaviour is a result of the negligible mean value of κ_m for statistically planar flames, which also leads to small values of the mean contribution of $-2\rho D\kappa_m|\nabla c|$. The contribution of $-2\rho D\kappa_m|\nabla c|$ is identically zero for planar unstretched laminar premixed flames, and thus, $\nabla\cdot(\rho D\nabla c)$ and $\vec{N}\cdot\left(\rho D\vec{N}\cdot\nabla c\right)$ remain identical in this case. It can further be seen from Figure 3 that the mean value of $[\dot{w} + \nabla\cdot(\rho D\nabla c)] = \rho S_d|\nabla c|$ remains close to the mean value of $\rho_0 S_L|\nabla c|$ for the turbulent flames when the flame is away from the wall (e.g., $t/t_f = 3.99$) and $[\dot{w} + \nabla\cdot(\rho D\nabla c)] = \rho S_d|\nabla c|$ is identical to $\rho_0 S_L|\nabla c|$ in the unstretched laminar premixed flame. The mean behaviours of $\dot{w}$, $\nabla\cdot(\rho D\nabla c)$, $\vec{N}\cdot\left(\rho D\vec{N}\cdot\nabla c\right)$, $-2\rho D\kappa_m|\nabla c|$, $[\dot{w} + \nabla\cdot(\rho D\nabla c)]$, and $\rho S_d|\nabla c|$ are found to be consistent with previous findings without the influence of walls (Chakraborty 2007; Chakraborty and Cant 2004, 2005, 2006).

Figure 3 indicates that the mean behaviour of $\dot{w}$ is not significantly affected by the presence of the wall in the case of adiabatic boundary condition but the mean value of $\dot{w}$ drops with time in the isothermal wall case, as the flame starts to quench due to heat loss through the wall. Moreover, the mean value of $|\nabla c|$ decreases with the progress of flame-wall interaction in the case of isothermal wall boundary condition, but this tendency remains negligible for the case with adiabatic wall boundary (see Figure 3). The detailed explanation for this behaviour has been provided elsewhere (Ahmed, Chakraborty, and Klein 2021c; Kai et al. 2022) and thus will not be repeated here. The drop in the value of $|\nabla c|$ gives rise to a decrease in the magnitude of the mean values of $\vec{N}\cdot\left(\rho D\vec{N}\cdot\nabla c\right) = -\partial(\rho D|\nabla c|)/\partial n$ with the progress of flame quenching in the case of isothermal walls. The magnitude of the mean value of $\vec{N}\cdot\left(\rho D\vec{N}\cdot\nabla c\right)$ also marginally decreases with time as the FWI progresses in the case of adiabatic wall boundary condition, but this trend is weaker than that in the case of isothermal wall boundary condition. Because of the wall-induced vortical motion, the probability of obtaining negative κ_m becomes higher than finding positive κ_m values when the flame reaches close to the wall and therefore the mean value of $-2\rho D\kappa_m|\nabla c|$ becomes positive at advanced stages of HOI (e.g., $t/t_f = 14.70$) in the case of adiabatic boundary condition. This marginally increases the magnitude of the positive contribution of $\nabla\cdot(\rho D\nabla c) = \vec{N}\cdot\left(\rho D\vec{N}\cdot\nabla c\right) - 2\rho D\kappa_m|\nabla c|$ towards the unburned gas side and acts to decrease the negative contribution of $\nabla\cdot(\rho D\nabla c)$ towards the burned gas side. As a result, the mean value of $[\dot{w} + \nabla\cdot(\rho D\nabla c)] = \rho S_d|\nabla c|$ increases with the progress of HOI in the adiabatic wall case.

Probability density functions (PDFs) of S^*_d/S_L and its components

The probability density functions (PDFs) of S^*_d/S_L and its components (i.e., S^*_r/S_L, S^*_n/S_L, and S^*_t/S_L) for the $c = 0.8$ isosurface at different stages of HOI are shown in Figure 4 for both isothermal and adiabatic wall boundary conditions. It can be seen from Figure 4 that S^*_d assumes predominantly positive values, as expected, when the flame remains away from the wall (e.g., $t/t_f = 3.99$) and thus is not affected by its presence. This is consistent with the previously obtained behaviour of the displacement speed in the corrugated flamelets regime

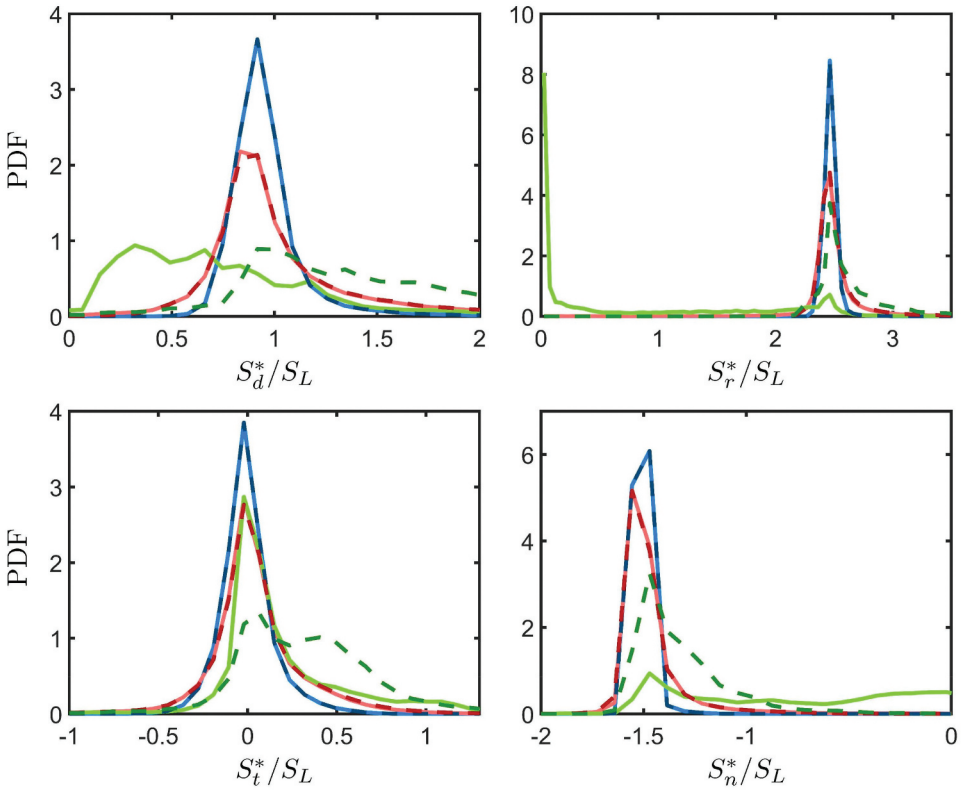

Figure 4. PDFs of S_d^*/S_L and its components (i.e., S_r^*/S_L, S_n^*/S_L, and S_t^*/S_L) for the $c = 0.8$ isosurface for adiabatic (dashed line) and isothermal (solid line) wall conditions at $t/t_r = 3.99$(blue), 10.92(red), 14.70(green).

(Chakraborty 2007). However, the width of the PDF of S_d^*/S_L increases with the progress of HOI. At $t/t_f = 14.70$, when the flame has interacted with the wall, the occurrence of higher positive values of S_d^*/S_L has a greater probability in the adiabatic wall case than in the isothermal wall boundary condition. To explain this behaviour, it is instructive to examine the PDFs of S_r^*/S_L, S_n^*/S_L, and S_t^*/S_L. It can be seen from Figure 4 that $S_t^*/S_L = -2D\kappa_m/S_L$ peaks at the zero value and exhibits an equal likelihood of positive and negative values for both isothermal and adiabatic boundary conditions at early times (e.g., $t/t_f = 3.99$) when the flame remains away from the wall. This is a consequence of the statistically planar nature of the flames considered here. However, the width of S_t^*/S_L PDFs increases with the progress of FWI, as the near-wall vortical structures tend to wrinkle the flames more as they come close to the wall. Moreover, the probability of finding positive values of S_t^*/S_L is greater than that for negative values for the adiabatic wall case when the flame is close to the wall (e.g., $t/t_f = 14.70$), which is consistent with positive mean values of $-2\rho D\kappa_m|\ c|$ during advanced stages of HOI (see Figure 3). The components S_r^*/S_L and S_n^*/S_L assume positive and predominantly negative values, respectively, at the flame surface, which is consistent with previous analyses (Chakraborty 2007, Ozel-Erol et al 2022; Chakraborty and Cant 2004, 2005; Echekki and Chen 1996, 1999; Peters et al. 1998). It can also be seen from Figure 4 that the probability of high positive values of S_r^*/S_L in the isothermal wall boundary

condition dramatically decreases with the progress of HOI and at later times (e.g., $t/t_f = 14.70$) a sharp peak of the S_r^*/S_L PDF is obtained at $S_r^*/S_L = 0$, which is indicative of the flame quenching as a result of wall heat loss. The normal diffusion component S_n^*/S_L can alternatively be written as: $S_n^* = -\vec{N} \cdot \quad (\rho D|\quad c|)/\rho_0|\quad c|$, which suggests that the statistical behaviour of $|\quad c|$ affects the distribution of S_n^*. It has been demonstrated elsewhere (Ahmed, Chakraborty, and Klein 2021c) that $|\quad c|$ assumes small values in the near-wall region and interested readers are referred to Ahmed, Chakraborty, and Klein (2021c) where detailed physical explanations were provided.

It is important to note that $|\quad c|$ is identically zero in the purely unburned and fully burned gases. Thus, the quantity $\left|\vec{N} \cdot \quad (|\quad c|)\right|$ scales as $\left|\vec{N} \cdot \quad (|\quad c|)\right| \sim \max(|\quad c|)/\delta$, where δ is the flame front thickness which can be taken to scale as: $\max(|\quad c|) \sim 1/\delta$ (Sankaran et al. 2007). This suggests $\left|\vec{N} \cdot \quad (|\quad c|)\right| \sim \max(|\quad c|)^2$, which acts to decrease $\left|S_n^*\right|$, as the HOI progresses with time. The combination of a decrease in the magnitudes of positive S_r^*/S_L and negative S_n^*/S_L acts to reduce the mean value of S_d^*/S_L with the progress of HOI for the isothermal wall case which can be substantiated by Table 1 where the mean values of S_d^*/S_L and its components for the $c = 0.8$ isosurface during the evolution of HOI are reported. For the adiabatic case, the increase in positive S_t^*/S_L with the progress of HOI gives rise to a mean value of S_d^*/S_L greater than unity, as the decrease in the values of $|\quad c|$ is negligible and $\dot{w}$ values remain comparable at different stages of HOI. Moreover, the increased width of S_t^*/S_L PDF owing to the flame wrinkling induced by near-wall vortical motion acts to increase the width of S_d^*/S_L PDF with the progress of HOI for both thermal boundary conditions. This can be substantiated by the standard deviations of S_d^*/S_L at different stages of HOI in Table 1. The flame quenching in the isothermal wall case gives rise to greater variations of S_r^* and S_n^* on the flame surface than that in the adiabatic wall boundary condition. This gives rise to wider PDFs of S_{r+n}^*/S_L in the isothermal wall case than in the case of the adiabatic wall, and this can be verified from the greater standard deviations of $S_{r+n}^*/S_L = \left(S_r^* + S_n^*\right)/S_L$ in the isothermal case in Table 1. This also contributes to the wider S_d^*/S_L PDFs in the isothermal wall case than that in the case of the adiabatic wall.

Local curvature and tangential strain rate dependence of in the case of HOI

In order to understand the local curvature κ_m and tangential strain rate $a_T = \left(\delta_{ij} - N_i N_j\right)\partial u_i/\partial x_j$ dependences of S_d^*, it is worth investigating the statistical variations of $|\quad c|$ in response to κ_m and a_T and interrelation between a_T and κ_m. The joint PDF contours

Table 1. The mean values (MV) and the standard deviations (SD) of S_d^*/S_L and its components on $c = 0.8$ isosurface with the progress of HOI for adiabatic (AW) and isothermal (IW) walls.

		S_d^*/S_L		S_t^*/S_L		S_n^*/S_L		S_r^*/S_L		S_{r+n}^*/S_L	
	t/t_f	MV	SD	MV	SD	MV	SD	MV	SD	MV	SD
AW	3.99	0.957	0.188	−0.002	0.149	−1.506	0.036	2.468	0.060	0.959	0.093
	10.92	1.107	0.613	0.045	0.309	−1.473	0.150	2.535	0.290	1.062	0.425
	14.70	1.700	1.050	0.332	0.466	−1.316	0.247	2.692	0.493	1.376	0.722
IW	3.99	0.957	0.188	−0.002	0.149	−1.509	0.036	2.468	0.060	0.959	0.093
	10.92	1.055	0.561	0.031	0.310	−1.465	0.178	2.488	0.306	1.023	0.377
	14.70	0.837	1.174	0.363	1.009	−0.263	1.097	0.803	0.985	0.564	0.857

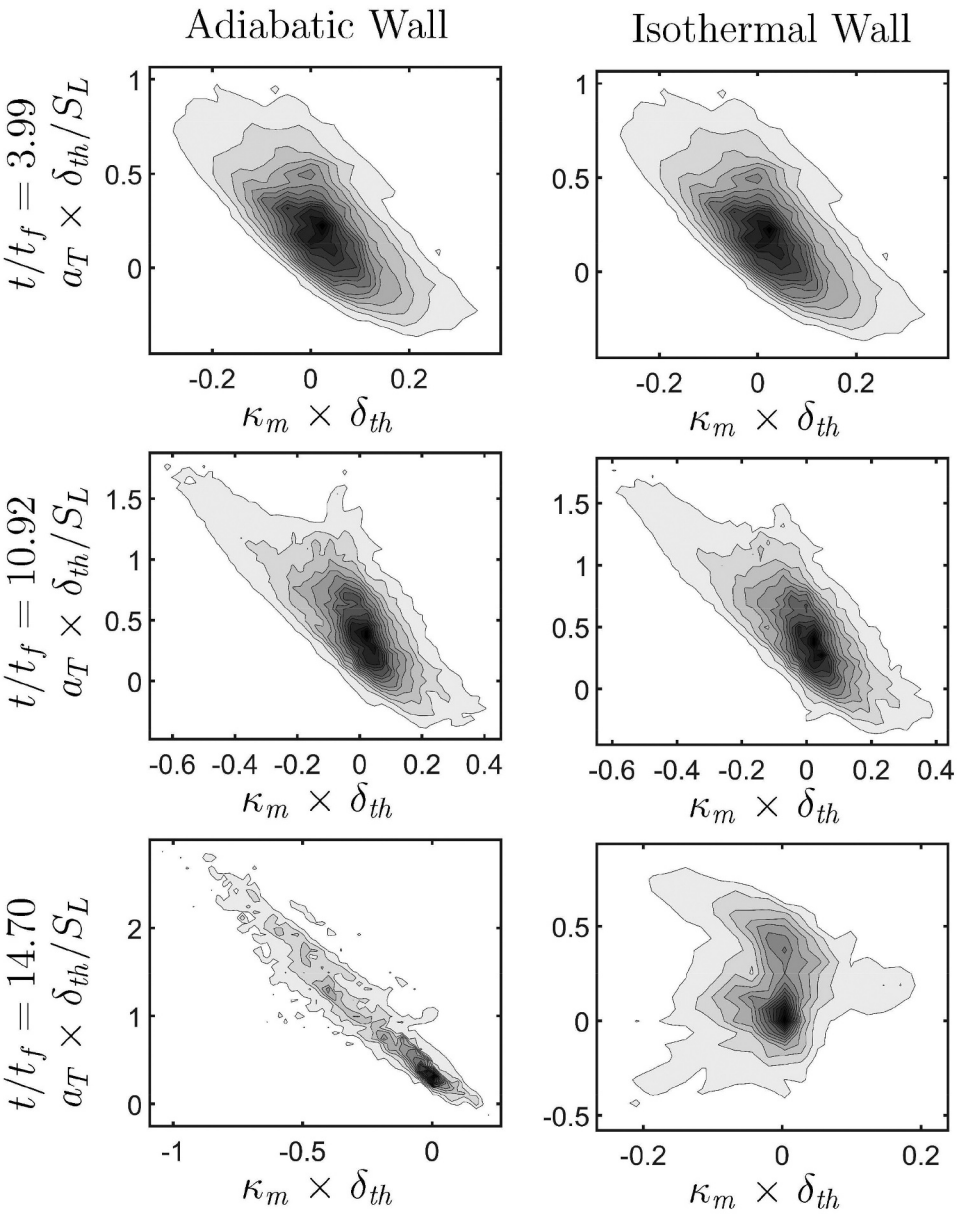

Figure 5. Contours of joint PDF between $a_T \times \delta_{th}/S_L$ and $\kappa_m \times \delta_{th}$ for the $c = 0.8$ isosurface at $t/t_f = 3.99(\text{top}), 10.92(\text{middle}), 14.70(\text{bottom})$ for adiabatic and isothermal walls.

between a_T and κ_m for the $c = 0.8$ isosurface at different stages of HOI are shown in Figure 5 for both isothermal and adiabatic wall boundary conditions and the corresponding correlation coefficients are listed in Table 2. It can be seen from Figure 5 that the correlation between a_T and κ_m remains negative for both cases but the correlation weakens as the flames approach the wall. The negative correlation between a_T and κ_m is consistent with several previous analyses without walls (Renou et al. 1998; Haworth and Poinsot 1992; Chakraborty and Cant 2004, 2005; Chakraborty 2007; Ozel-Erol et al 2022). The negative correlation between a_T and κ_m

Table 2. Correlations coefficients on $c = 0.8$ isosurface with the progress of HOI for adiabatic (AW) and isothermal (IW) walls. Correlation coefficients between quantities x and y are calculated as: $R_{xy} = \left[\sum_i x_i y_i - N\bar{x}\bar{y}\right] / \left[\sqrt{\sum_i x_i^2 - N\bar{x}^2}\sqrt{\sum_i y_i^2 - N\bar{y}^2}\right]$. Here, x_i, y_i are individual sample points, N is sample size, and $\bar{x}, \bar{y}$ are the mean values for a given value of c-isosurface.

	t/t_f	$a_T - \kappa_m$	$\lvert c\rvert - a_T$	$\lvert c\rvert - \kappa_m$	$S^*_{r+n} - a_T$	$S^*_r - a_T$	$S^*_n - a_T$	$S^*_{r+n} - \kappa_m$	$S^*_t - a_T$	$S^*_d - a_T$	$S^*_d - \kappa_m$	$S^*_d - K$
AW	3.99	−0.792	0.182	0.036	−0.093	−0.216	0.119	−0.161	0.791	0.582	−0.873	−0.966
	10.92	−0.526	0.063	0.340	−0.015	−0.065	0.083	−0.383	0.484	0.234	−0.694	−0.620
	14.70	−0.532	−0.291	0.588	0.163	0.108	0.265	−0.507	0.320	0.270	−0.682	−0.375
IW	3.99	−0.792	0.182	0.036	−0.093	−0.216	0.119	−0.161	0.791	0.582	−0.873	−0.966
	10.92	−0.577	0.153	0.157	0.028	0.066	−0.052	−0.376	0.542	0.318	−0.704	−0.608
	14.70	−0.029	0.316	0.348	0.048	0.371	−0.297	−0.026	−0.014	0.011	−0.269	−0.290

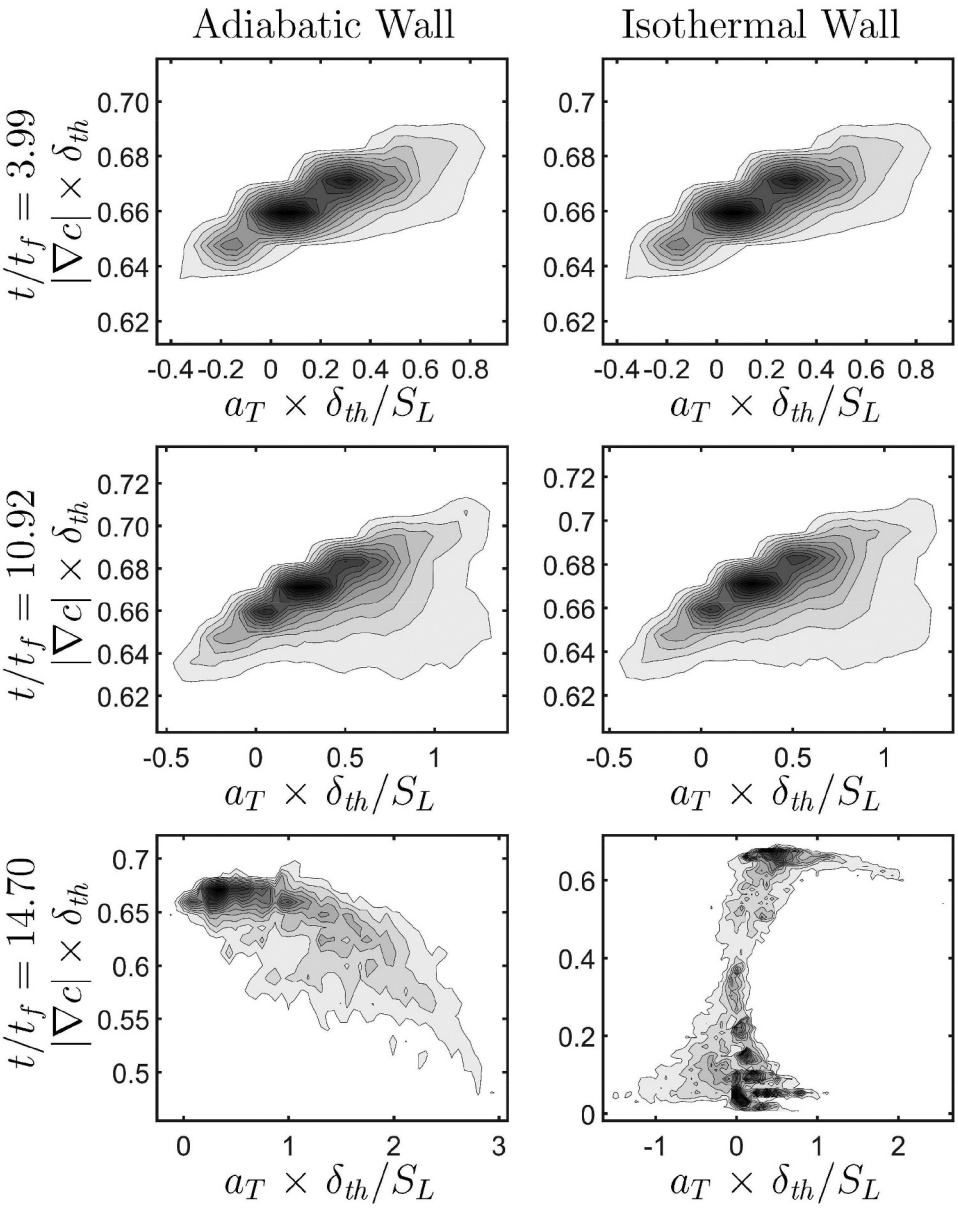

Figure 6. Contours of joint PDF between $|\nabla c| \times \delta_{th}$ and $a_T \times \delta_{th}/S_L$ for the $c = 0.8$ isosurface at $t/t_f = 3.99$(top), 10.92(middle), 14.70(bottom) for adiabatic and isothermal walls.

arises principally due to thermal expansion but these effects weaken in the vicinity of the wall because the flame experiences strong fluid-dynamic straining due to the shear rate induced by the wall which is largely independent of flame curvature. Moreover, in the case of isothermal wall boundary conditions, the flame quenching due to wall heat loss weakens the effects of thermal expansion in the vicinity of the wall which leads to a negligible correlation coefficient between a_T and κ_m at $t/t_f = 14.70$ (Table 2).

The interrelation between a_T and κ_m also affects the strain rate and curvature dependences of $|\ c|$. The contours of joint PDFs between $|\ c|$ and a_T for the $c = 0.8$ isosurface at different stages of HOI are shown in Figure 6 for both isothermal and adiabatic wall boundary conditions. The corresponding correlations are provided in Table 2. It can be seen from Figure 6 and Table 2 that $|\ c|$ and a_T are weakly positively correlated away from the wall (e.g., $t/t_f = 3.99$) and the correlation remains positive as the flame approaches the flame for the isothermal wall case. The correlation between $|\ c|$ and a_T remains positive when the flame is away from the wall in the adiabatic wall boundary case with a comparable correlation strength as that in the isothermal wall case. In the case of adiabatic wall boundary conditions, the correlation between $|\ c|$ and a_T becomes negative as time progresses. In order to explain the aforementioned behaviour, it is worthwhile to consider the following relation:

$$a_T + a_n = \partial u_i/\partial x_i \tag{7}$$

where $a_n = N_i N_j \partial u_i/\partial x_j$ is the normal strain rate. The PDFs of $a_T \times \delta_{th}/S_L$ and $\partial u_i/\partial x_i \times \delta_{th}/S_L$ for the $c = 0.8$ isosurface at different time instants are shown in Figures 7 and 8, respectively. It can be seen from Figure 8 that the probability of high positive values of $\partial u_i/\partial x_i$ decreases as the flame comes in the vicinity of the wall in the case of isothermal wall boundary condition. For the isothermal wall boundary condition, flame quenching in the vicinity of the wall gives rise to the weakening of thermal expansion, which leads to a significant reduction in the probabilities of finding high positive values of $\partial u_i/\partial x_i$ with a strong peak at zero value. The increased probability of finding negative curvatures at later times in the case of adiabatic boundary conditions gives rise to an increased probability of high dilatation rates due to the focusing of heat at the negatively curved zones. It is important to appreciate that the magnitude of $\partial u_i/\partial x_i$ is principally determined by the thermo-chemistry, whereas a_T is principally determined by the background fluid motion (i.e., turbulence).

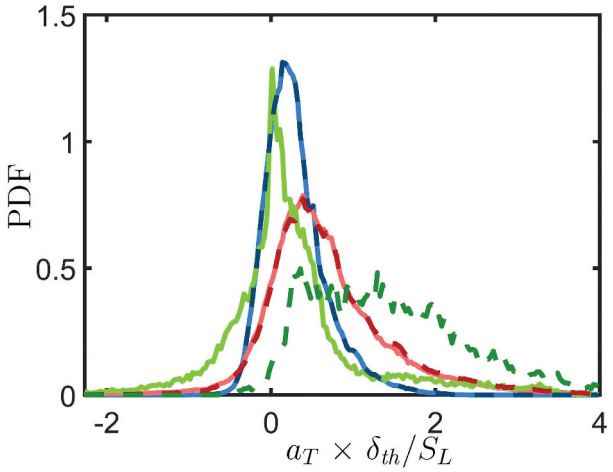

Figure 7. PDFs of $a_T \times \delta_{th}/S_L$ for the $c = 0.8$ isosurface for adiabatic (dashed line) and isothermal (solid line) wall conditions at $t/t_f = 3.99(\text{blue}), 10.92(\text{red}), 14.70(\text{green})$.

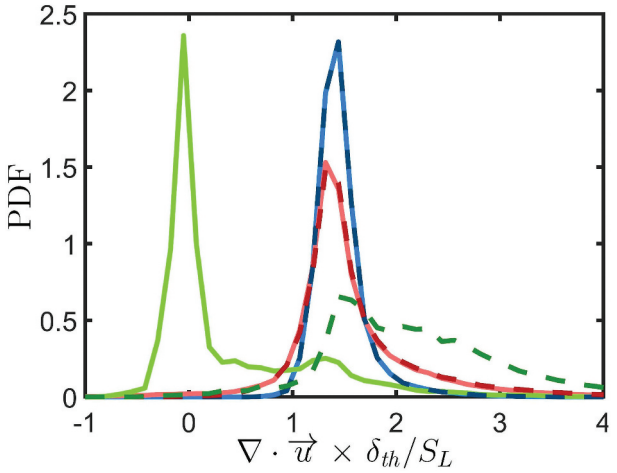

Figure 8. PDFs of $(\partial u_i/\partial x_i) \times \delta_{th}/S_L$ for the $c = 0.8$ isosurface for adiabatic (dashed line) and isothermal (solid line) wall conditions at $t/t_f = 3.99(\text{blue}), 10.92(\text{red}), 14.70(\text{green})$.

As a_T is representative of fluid-dynamic straining due to turbulence, an increase in a_T in comparison to $\partial u_i/\partial x_i$ gives rise to a decrease in a_n when the flame remains away from the wall (e.g., $t/t_f = 3.99$). Under the action of the decreasing trend of a_n, the isoscalar lines tend to come close to each other, which acts to increase $|\nabla c|$, which has been shown earlier for FWI in fully developed channel flows by Ahmed et al (2020, 2021a). This gives rise to a positive correlation between $|\nabla c|$ and a_T away from the wall, which is consistent with several previous analyses (Chakraborty and Cant 2005; Chakraborty and Klein 2008; Chakraborty, Klein, and Cant 2007). When the flame starts to quench in the case of isothermal boundary condition, $\partial u_i/\partial x_i$ becomes small before assuming negligible values when the flame is fully quenched. Under this condition, an increase in a_T leads to a decrease in a_N, which acts to increase $|\nabla c|$. Thus, a positive correlation between $|\nabla c|$ and a_T is observed at all stages for flame-wall interaction in the case of isothermal wall boundary conditions.

In the case of adiabatic wall boundary condition, an increase in a_T in the negatively curved regions due to the negative correlation between a_T and κ_m (see Figure 5) is also associated with the increased value of $\partial u_i/\partial x_i$ due to the focusing of diffusive heat flux. If the increase in $\partial u_i/\partial x_i$ overcomes that of a_T in the negatively curved regions when the flame is close to the wall, an increase in a_T also gives rise to an increase in a_N, which acts to decrease $|\nabla c|$. This leads to negative correlations between $|\nabla c|$ and a_T when the flame comes close to the wall (e.g., $t/t_f = 10.92$ and 14.70) in the case of adiabatic wall boundary conditions.

The contours of joint PDFs between $|\nabla c|$ and κ_m for the $c = 0.8$ isosurface at different stages of HOI are shown in Figure 9 and the corresponding correlation coefficients are listed in Table 2. It can be seen from Figure 9 that $|\nabla c|$ and κ_m remain weakly correlated at all stages of HOI in the isothermal wall boundary conditions. However, the correlation becomes increasingly positive with the progress of HOI in the case of adiabatic wall boundary condition. This is a consequence of $\partial u_i/\partial x_i$ overcoming a_T in the negatively curved regions which gives rise to an

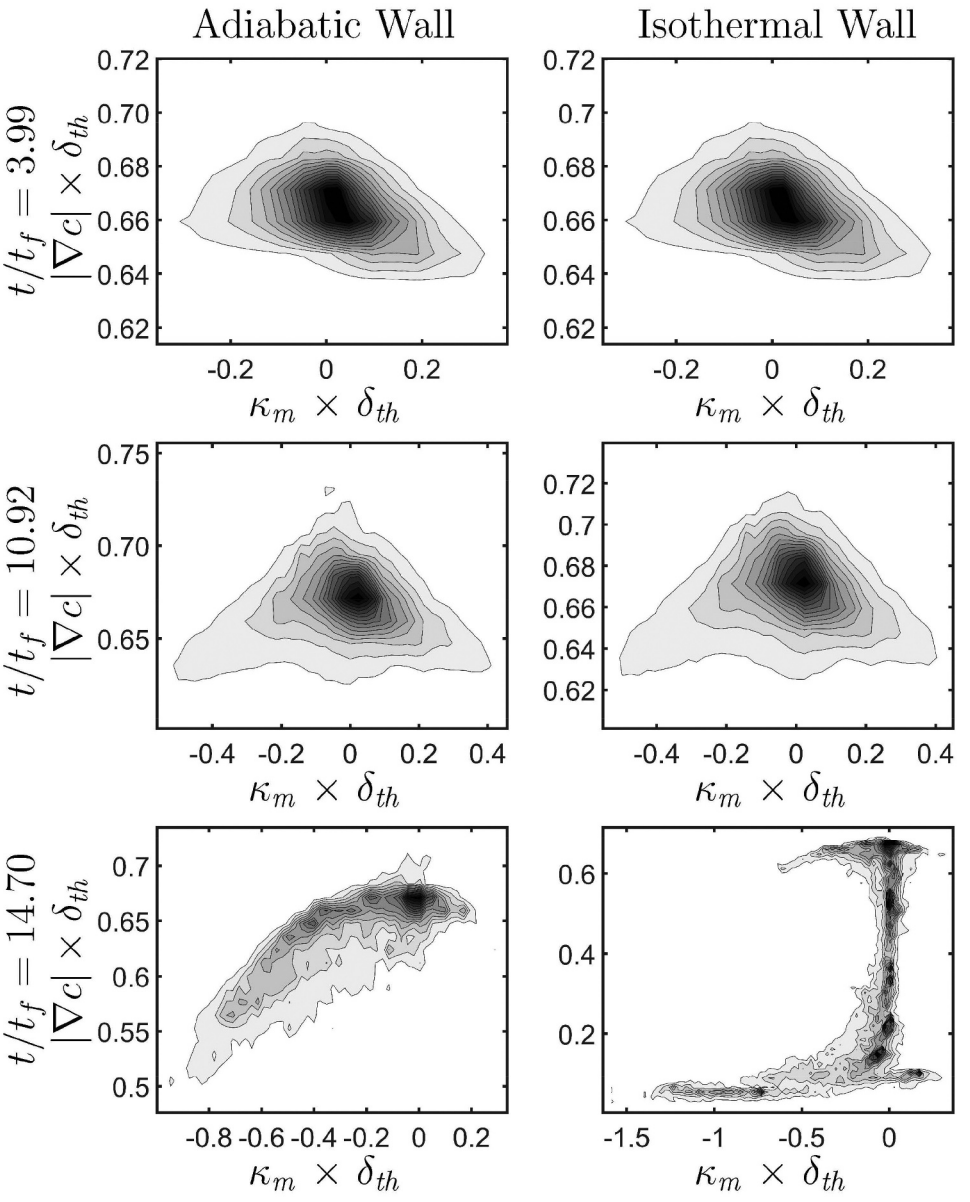

Figure 9. Contours of joint PDF between $|\nabla c| \times \delta_{th}$ and $\kappa_m \times \delta_{th}$ for the $c = 0.8$ isosurface at $t/t_f = 3.99$(top), 10.92(middle), 14.70(bottom) for adiabatic and isothermal walls.

increase in a_N and therefore acts to decrease $|\nabla c|$. The combination of positive correlation between $|\nabla c|$ and a_T and negative correlation between a_T and κ_m gives rise to the negatively correlating branch in the joint PDF between $|\nabla c|$ and κ_m when the flame remains away from the wall. Due to the focusing of diffusive heat flux at the negatively curved regions, the dilatation rate $\partial u_i/\partial x_i$ can locally assume higher values than the tangential strain rate a_T and induce extensive normal strain rate a_n,

which acts to reduce the magnitude of $|\ c|$. This gives rise to a positively correlating branch between $|\ c|$ and κ_m in the negatively curved zones when the flame is away from the wall. This behaviour is found to be consistent with several previous analyses (Chakraborty and Cant 2004, 2005; Chakraborty, Klein, and Cant 2007; Chakraborty and Klein 2008; Chakraborty et al. 2008; Keil et al. 2021a, 2021b).

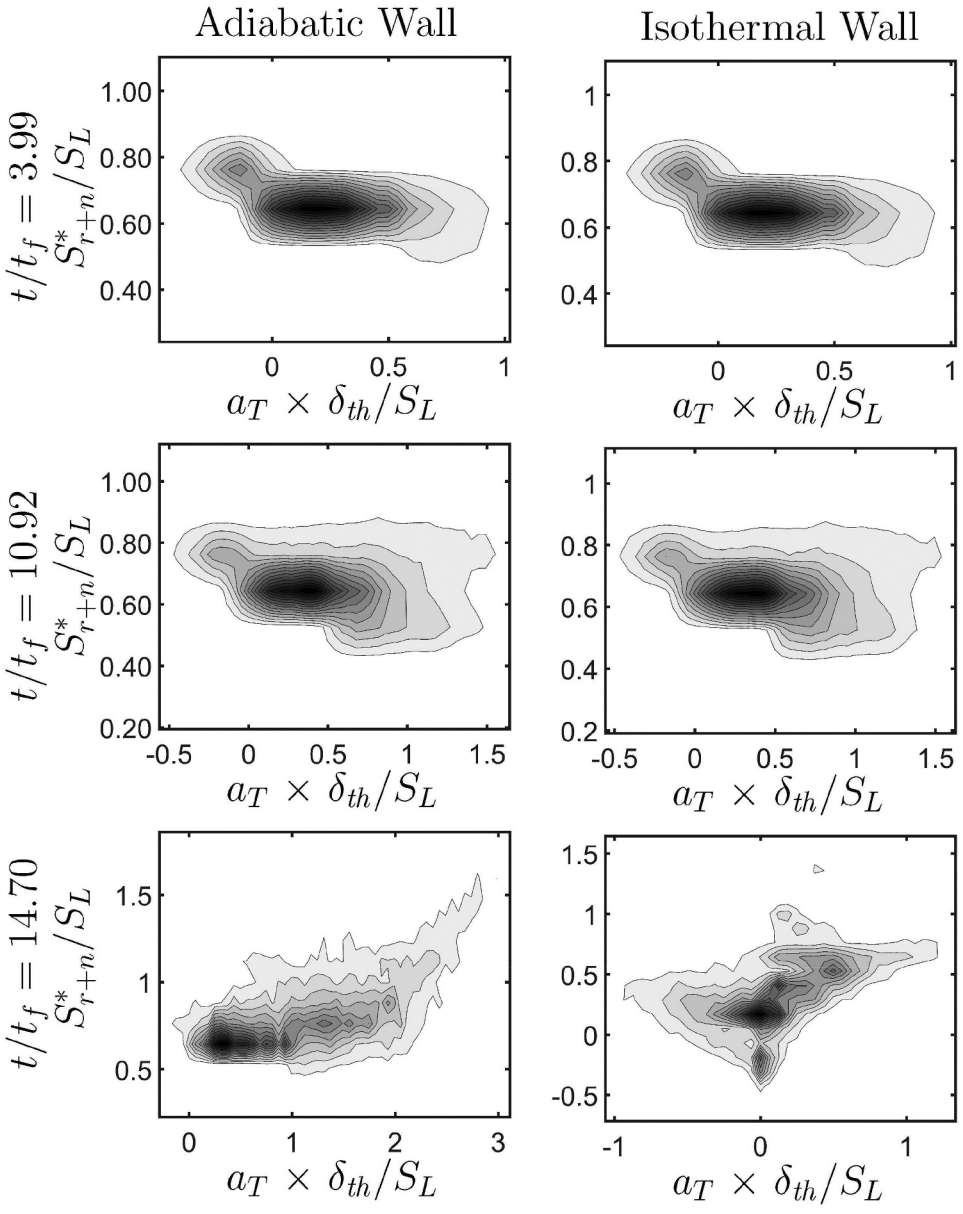

Figure 10. Contours of joint PDF between $S^*_{r+n}/S_L = \left(S^*_r + S^*_n\right)/S_L$ and $a_T \times \delta_{th}/S_L$ for the $c = 0.8$ isosurface at $t/t_f = 3.99(\text{top}), 10.92(\text{middle}), 14.70(\text{bottom})$ for adiabatic and isothermal walls.

Local curvature and tangential strain rate dependence of S^*_d and its components in the case of HOI

The strain rate and curvature dependences of $|\ \ c|$ affect the strain rate and curvature dependences of $S^*_{r+n} = \left(S^*_r + S^*_n\right)$. The contours of joint PDFs between $S^*_{r+n} = \left(S^*_r + S^*_n\right)$ and a_T for the $c = 0.8$ isosurface at different stages of HOI are shown in Figure 10 for both isothermal and adiabatic wall boundary conditions and the correlation coefficients are reported in Table 2. Both Table 2 and Figure 10 indicate that S^*_{r+n} remains weakly correlated with a_T when the flame is away from the wall. For low Mach number flows, $\dot{w}$ for a given value of c remains independent of a_T when the flame is away from the wall for unity Lewis number conditions. Thus, the positive correlation between $|\ \ c|$ and a_T induces a negative correlation between S^*_r and a_T according to Equation 4 when the flame is away from the wall. The normal diffusion component of density-weighted displacement speed S^*_n can be scaled as $\vec{N}\cdot\ \ \cdot\left(\rho D\vec{N}\cdot\ \ c\right) \sim \left(\rho D/\rho_0|\ \ c|\right)\partial^2 c/\partial n^2$. As $\left(\rho D/\rho_0|\ \ c|\right)\partial^2 c/\partial n^2$ is predominantly negative in the reaction zone (Chakraborty and Cant 2004, 2005; Chakraborty 2007; Keil et al. 2021a, 2021b; Ozel-Erol et al 2022), the net effect of positive correlation between $|\ \ c|$ and a_T induces a weak positive correlation between S^*_n and a_T. This positive correlation between S^*_n and a_T is partially nullified by the negative correlation between S^*_r and a_T to yield a weak correlation between S^*_{r+n} and a_T when the flame is away from the wall. The correlation coefficients between S^*_r and a_T and between S^*_n and a_T remain close in magnitude but have opposite signs (except for the adiabatic wall condition at $t/t_f = 14.70$ but correlations remain weak) and therefore the net correlation between S^*_{r+n} and a_T remains weak (e.g., $t/t_f = 10.92$ and 14.70) throughout FWI in this case.

Both positive and negative correlation branches in the joint PDF between $|\ \ c|$ and κ_m (see Figure 9) give rise to two branches of comparable strength in the joint PDFs between S^*_{r+n} and κ_m when the flame is away from the wall, which can be substantiated by Figure 11 where the contours of joint PDFs between S^*_{r+n} and κ_m for the $c = 0.8$ isosurface at different stages of HOI are shown. Figure 11 indeed shows a weak correlation between S^*_{r+n} and κ_m, when the flame is away from the wall (e.g., $t/t_f = 3.99$), for both wall boundary conditions. The combination of a weak positive correlation between S^*_{r+n} and a_T and the negative correlation between a_T and κ_m leads to a weak negative correlation between S^*_{r+n} and κ_m at the advanced stage of HOI for isothermal boundary condition (see Figure 11 and Table 2). However, a significant negative correlation between S^*_{r+n} and κ_m is obtained when the flame is close to the adiabatic wall as a consequence of the combination of a stronger positive correlation between S^*_{r+n} and a_T and a stronger negative correlation between a_T and κ_m than in the isothermal wall case.

The component $S^*_t = -2\rho D\kappa_m/\rho_0$ is deterministically negatively correlated with κ_m with a correlation coefficient of −1.0 at all stages of HOI under both wall boundary conditions. The combination of negative correlations between S^*_t and κ_m and between a_T and κ_m gives rise to a positive correlation between S^*_t and a_T when the flame is away from the wall. However, the strength of the negative correlation between a_T and κ_m weakens with the progress of HOI, and thus, the positive correlation strength between S^*_t and a_T also weakens with time. The combination

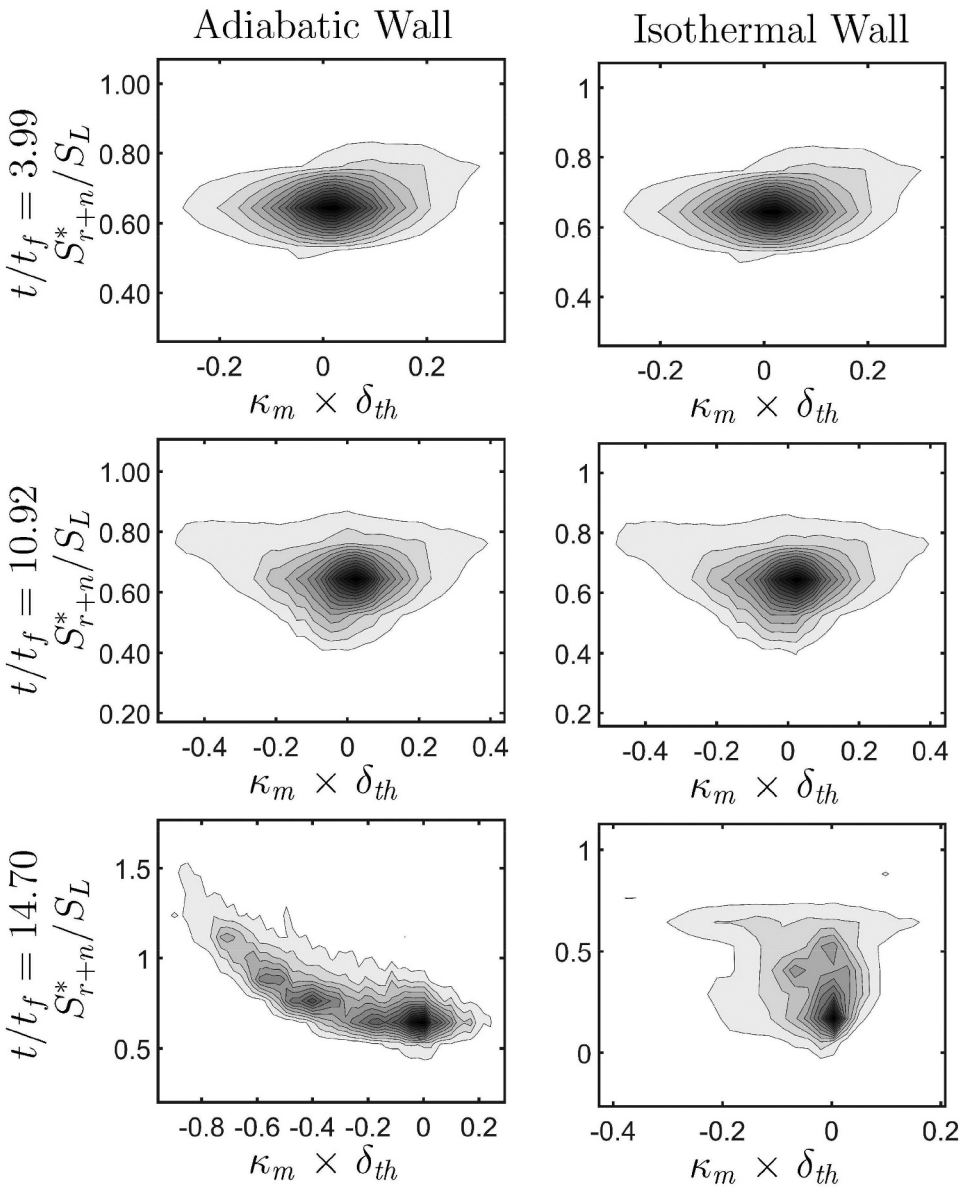

Figure 11. Contours of joint PDF between $S^*_{r+n}/S_L = \left(S^*_r + S^*_n\right)/S_L$ and $\kappa_m \times \delta_{th}$ for the $c = 0.8$ isosurface at $t/t_f = 3.99(\text{top}), 10.92(\text{middle}), 14.70(\text{bottom})$ for adiabatic and isothermal walls.

of positive correlations between S^*_t and a_T and mostly weak positive correlations between S^*_{r+n} and a_T gives rise to a positive correlation between S^*_d and a_T at all stages of HOI for both boundary conditions (see Table 2), which can be substantiated by Figure 12 where the contours of joint PDFs between S^*_d and a_T for the $c = 0.8$ isosurface at different stages of HOI for both boundary conditions. The correlation coefficient between S^*_d and a_T (i.e., $corr\left(S^*_d, a_T\right)$) can be expressed as (Chakraborty and Cant 2005):

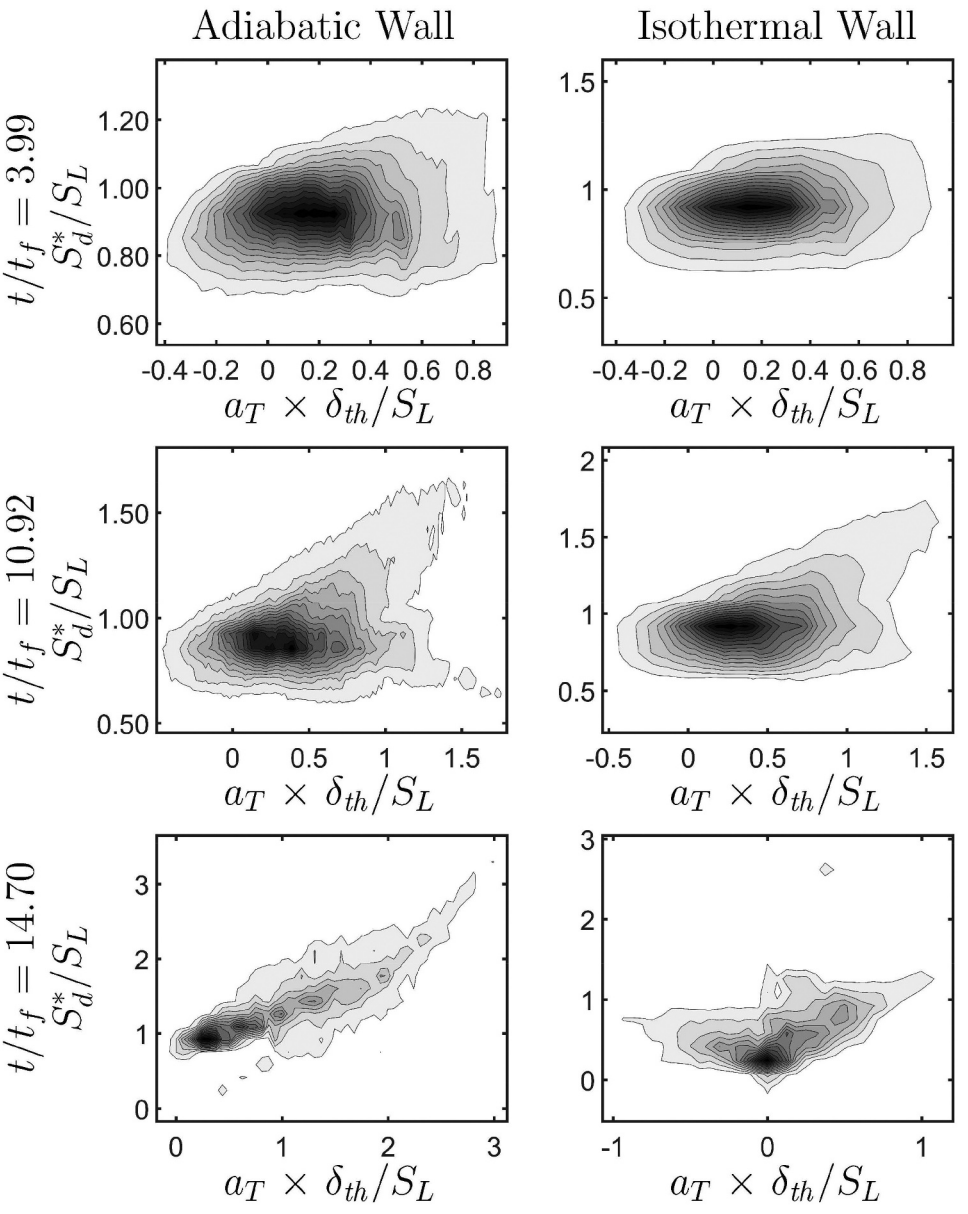

Figure 12. Contours of joint PDF between S_d^*/S_L and $a_T \times \delta_{th}/S_L$ for the $c = 0.8$ isosurface at $t/t_f = 3.99$(top), 10.92(middle), 14.70(bottom) for adiabatic and isothermal walls.

$$corr\left(S_d^*, a_T\right) = \frac{Corr\left(S_{r+n}^*, a_T\right) SD\left(S_{r+n}^*\right) + Corr\left(S_t^*, a_T\right) SD\left(S_t^*\right)}{SD\left(S_d^*\right)} \tag{8}$$

where $corr(q_1, q_2)$ is the correlation coefficient between q_1 and q_2, and $SD(q_1)$ is the standard deviation of q_1. Equation 8 indicates that the relative magnitudes of $SD\left(S_d^*\right)$, $SD\left(S_{r+n}^*\right)$, and $SD\left(S_t^*\right)$ along with $Corr\left(S_{r+n}^*, a_T\right)$ and $Corr\left(S_t^*, a_T\right)$ determine the correlation strength between S_d^* and a_T. Under both boundary conditions the value of

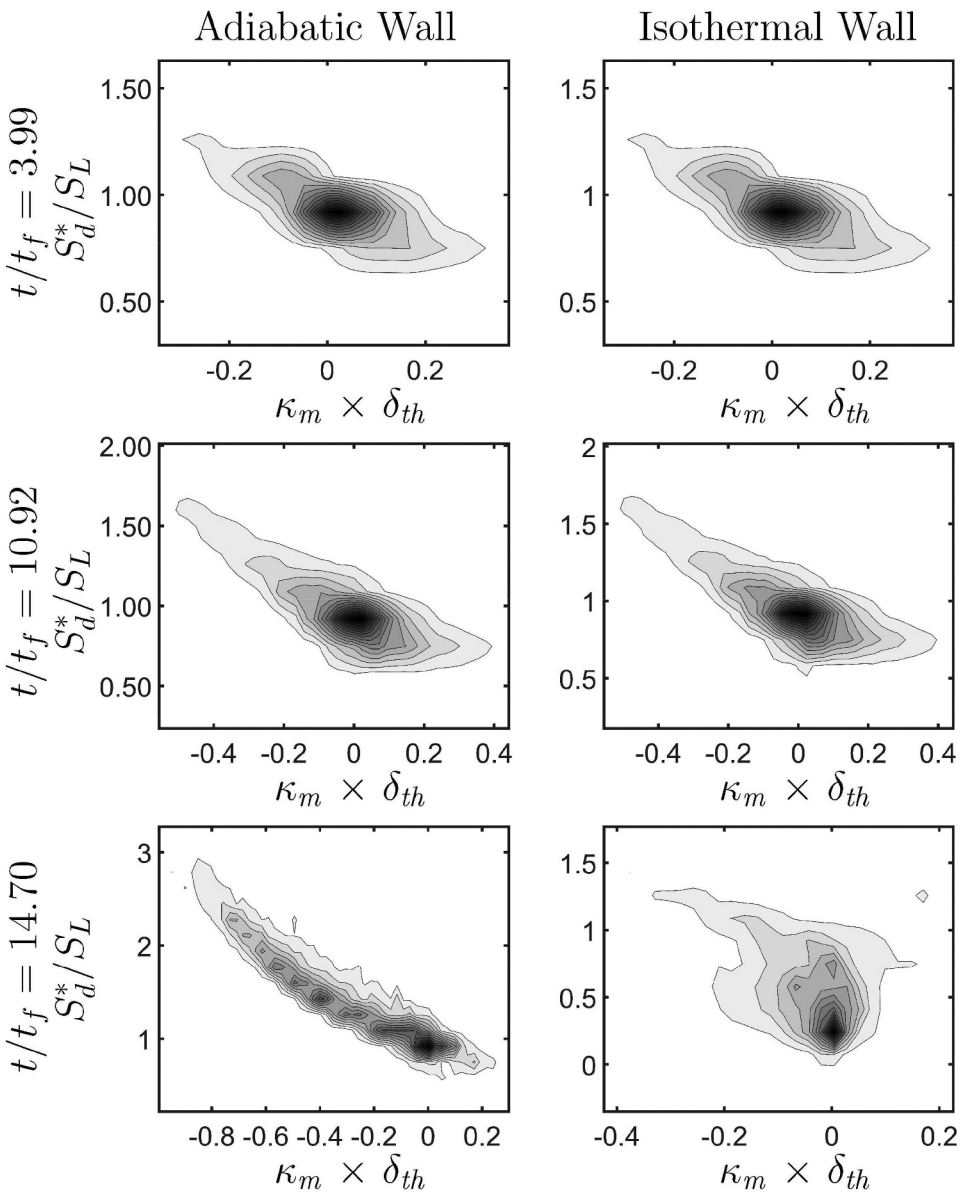

Figure 13. Contours of joint PDF between S_d^*/S_L and $\kappa_m \times \delta_{th}$ for the $c = 0.8$ isosurface at $t/t_f = 3.99$(top), 10.92(middle), 14.70(bottom) for adiabatic and isothermal walls.

$corr(S_d^*, a_T)$ decreases with the progress of HOI. The higher value of $SD(S_d^*)$ at the advanced stages of HOI (e.g., $t/t_f = 14.70$) in the isothermal wall case acts to yield a smaller value of $corr(S_d^*, a_T)$ than that in the case of adiabatic wall boundary condition.

The deterministically negative correlation between S_t^* and κ_m with a correlation coefficient of −1.0 principally gives rise to the negative correlation between S_d^* and κ_m at all times for both wall boundary conditions. However, both positive and negative correlating

branches between S^*_{r+n} and κ_m give rise to a negative correlation between S^*_d and κ_m with a correlation coefficient significantly different from −1.0, which can be substantiated by Figure 13 where the contours of joint PDFs between S^*_d and κ_m for the $c = 0.8$ isosurface at different stages of HOI are shown for both thermal boundary conditions. Following Equation 8, the correlation coefficient between S^*_d and κ_m (i.e., $corr\left(S^*_d, \kappa_m\right)$) can be expressed as (Chakraborty and Cant 2005):

$$corr\left(S^*_d, \kappa_m\right) = \frac{Corr\left(S^*_{r+n}, \kappa_m\right) SD\left(S^*_{r+n}\right) + Corr\left(S^*_t, \kappa_m\right) SD\left(S^*_t\right)}{SD\left(S^*_d\right)} \tag{9}$$

It has also been demonstrated earlier (see Figure 4) that both $SD\left(S^*_{r+n}\right)$ and $SD\left(S^*_t\right)$ increase with the progress of HOI, which affect the correlation between S^*_d and κ_m, as the relative magnitudes of $SD\left(S^*_d\right)$, $SD\left(S^*_{r+n}\right)$, and $SD\left(S^*_t\right)$, along with $Corr\left(S^*_{r+n}, \kappa_m\right)$ and $Corr\left(S^*_t, \kappa_m\right)$, determine the negative correlation strength between S^*_d and κ_m. It has been found that the negative correlation between S^*_d and κ_m weakens with the progress of HOI (see Table 2). This weakening of the negative correlation between S^*_d and κ_m is relatively stronger for the isothermal boundary condition than in the adiabatic wall boundary condition (see Table 2). The higher values of $SD\left(S^*_d\right)$ (i.e., wider PDF of S^*_d in Figure 4) and $SD\left(S^*_{r+n}\right)$ in the isothermal boundary condition at the advanced stages of HOI (e.g., $t/t_f = 14.70$) act to reduce the magnitude of the negative correlation coefficient $Corr\left(S^*_d, \kappa_m\right)$ at later times according to Equation 9.

Finally, the contours of joint PDFs between S^*_d and stretch rate $K = a_T + 2\left(\rho_0/\rho\right)S^*_d\kappa_m$ for the $c = 0.8$ isosurface at different stages of HOI shown for both thermal boundary conditions are shown in Figure 14, which indicates a non-linear K dependence of S^*_d in agreement with previous analyses (Chen and Im 1998, Chen and Im, 2000; Chakraborty, Klein, and Cant 2007; Herbert et al. 2020; Chakraborty et al. 2022) for positive values of S^*_d. The contours of the joint PDFs shown in Figure 14 suggest that the stage of HOI alters the non-linear nature of K dependence of S^*_d and weakens the strength of the correlation (see Table 2). The weakening of curvature dependence of S^*_d with the progress of HOI (see Table 2) weakens the non-linear stretch rate dependence of S^*_d, which can be substantiated by the contours of joint PDFs between S^*_d and K in Figure 14.

Modelling implications

Using Equation. 3, it is possible to obtain the following relation (Boger et al. 1998; Trouvé and Poinsot 1994):

$$\overline{\dot{w}} + \overline{\nabla \cdot (\rho D \nabla c)} = \rho_0 \overline{\left(S^*_d\right)}_s \Sigma_{gen} \tag{10}$$

where $\bar{q}$ and $\overline{(q)}_s = \overline{q|\ \ c|}/\Sigma_{gen}$ are the Reynolds averaged/LES filtered and surface averaged/filtered values of q, respectively (Boger et al. 1998; Trouvé and Poinsot 1994), as appropriate. Figures 5, 6, 12, 13 and 14 indicate that both S^*_d and $|\ \ c|$ are affected by local variations of a_T, κ_m, and K, which suggest that it is not possible to consider a constant value of $\overline{\left(S^*_d\right)}_s$ for the closure of $\overline{\dot{w}} + \overline{\ \ \cdot (\rho D\ \ c)}$. Furthermore, it was demonstrated elsewhere (Chakraborty and Cant 2007, 2009) that the closure of $\overline{\left(S^*_d\right)}_s$ is not only needed for the

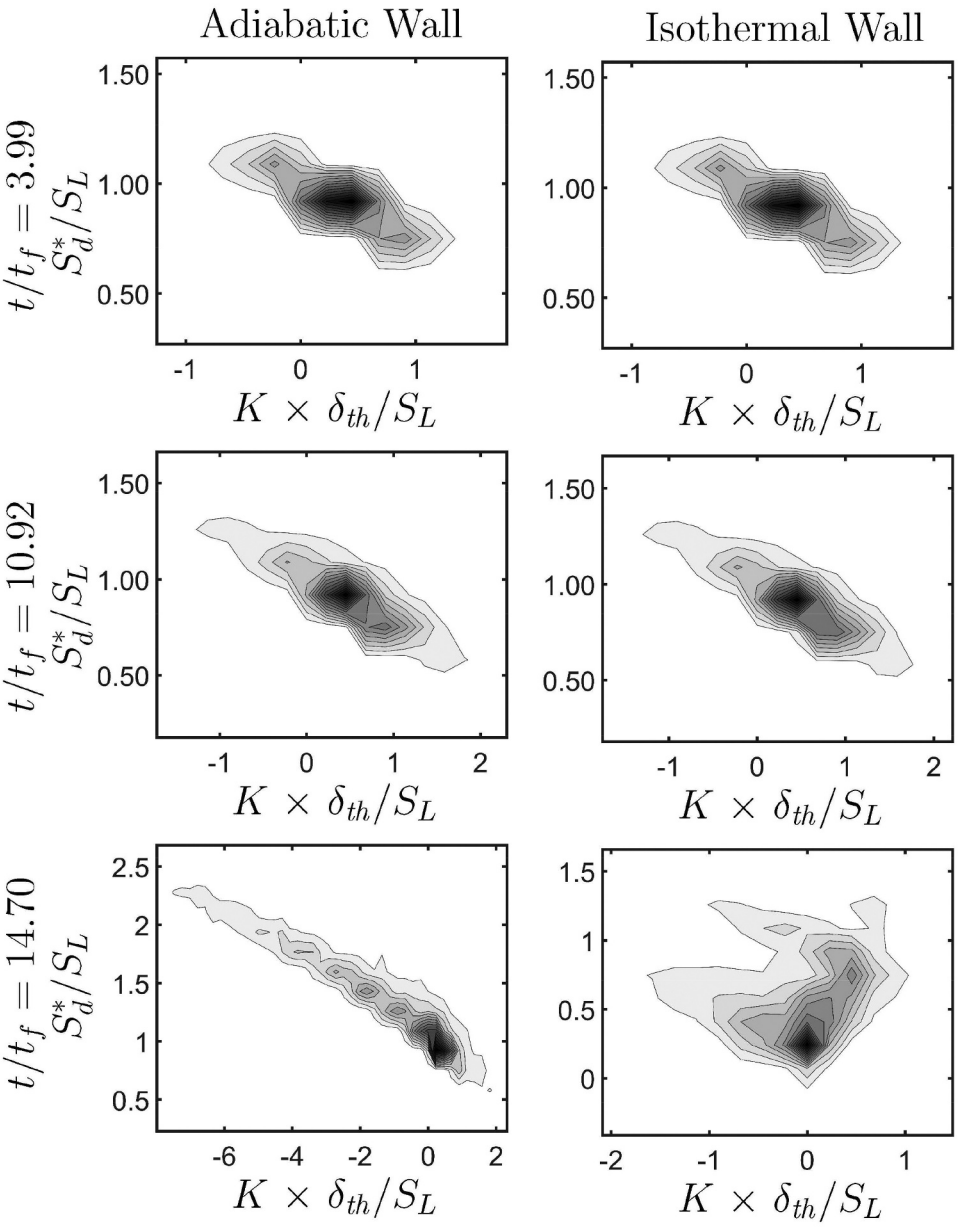

Figure 14. Contours of joint PDF between S_d^*/S_L and $K \times \delta_{th}/S_L$ for the $c = 0.8$ isosurface at $t/t_f = 3.99$(top), 10.92(middle), 14.70(bottom) for adiabatic and isothermal walls.

closure of $\overline{\dot{w}} + \overline{\quad \cdot (\rho D \quad c)}$ but also for the modelling of the unclosed terms in the transport equation of Σ_{gen}, especially for the curvature stretch contribution (i.e., $\overline{2(S_d\kappa_m)_s\Sigma_{gen}}$) to the FSD transport equation (Chakraborty and Cant 2007, 2009). The findings of the current analysis suggest that a_T and κ_m dependences of S_d^* need to be captured accurately to model the progress of HOI with time and also to account for the effects of thermal wall boundary conditions. It was demonstrated by Ghai et al. (2022) that the closure of $\overline{\dot{w}}$ in flame-wall

interaction in turbulent boundary layers is closely related to the wall heat transfer rate for isothermal wall boundary conditions and thus it will be necessary to have a high-fidelity model of $\overline{(S_d^*)}_s$, which includes local strain rate and curvature dependences, in the framework hybrid RANS/LES modeling of FWI in turbulent boundary layers to have accurate predictions of mean burning rate and wall heat transfer rate.

Conclusions

Three-dimensional DNS data of head-on interaction (HOI) of statistically planar premixed flames with a chemically inert wall across a turbulent boundary layer have been considered to investigate the statistics of density-weighted displacement speed S_d^* and its components for both isothermal and adiabatic wall boundary conditions. The PDFs of S_d^* have been found to widen with the progress of HOI. Dependencies of displacement speed to flame curvature and tangential strain rate are significantly affected by the presence of the wall and the type of thermal wall boundary condition. The increased variance of the tangential diffusion component of displacement speed S_t^* with the progress of HOI has been found to contribute to the widening of S_d^* PDFs with the progress of HOI. This widening of S_d^* PDFs is more prevalent in the case of isothermal wall boundary conditions than in the adiabatic wall case. The interaction between near-wall vortical structures and the flame surface can give rise to increased flame wrinkling when the flame comes in the vicinity of the wall for both thermal wall boundary conditions. This is reflected in the increased range of curvature κ_m variation with the progress of FWI, which is reflected in the widening of $S_t^* = -2\rho D\kappa_m/\rho_0$ PDFs. The thermal boundary condition directly affects the statistical behaviour of the reaction component of S_d^* (i.e., S_r^*) because the flame quenches when it comes close to the wall due to heat loss in the case of the isothermal wall, whereas the flame eventually extinguishes once all the reactants are consumed. As a result of this, the variations of both reaction rate $\dot{w}$ and the magnitude of reaction progress variable gradient $|\nabla c|$ are responsible for the distribution of S_r^* in the case of the isothermal wall, whereas the variation of S_r^* in the case of the adiabatic wall occurs due to $|\nabla c|$ variation. Thus, the PDF of S_r^* in the case of the isothermal boundary condition is wider than that in the case of the adiabatic wall boundary condition. This also contributes to the wider PDF of the combined reaction and normal diffusion component of S_d^* (i.e., $S_{r+n}^* = S_r^* + S_n^*$) and density-weighted displacement speed S_d^* in the case of the isothermal wall than that in the case of the adiabatic boundary condition.

The flame quenching in the case of the isothermal wall weakens the effects of dilatation rate and flame normal acceleration in comparison to those in the case of adiabatic wall boundary conditions. These effects are responsible for the differences in strain rate and curvature dependences of $|\nabla c|$ and the interrelation between a_T and κ_m for different boundary conditions during HOI. These aspects also give rise to quantitative differences in the correlations of S_{r+n}^* and S_t^* with tangential strain rate a_T and flame curvature κ_m for different wall boundary conditions. It has been found that the negative correlation coefficient between S_d^* and flame curvature κ_m decreases with the progress of HOI and the widening of S_{r+n}^* PDFs contributes to it for both wall boundary conditions. Similarly, the correlation coefficient between S_d^* and a_T also decreases with the progress of HOI for both thermal boundary conditions. The weakening of κ_m dependence of S_d^* with the progress of

HOI also gives rise to the weakening of stretch rate dependence of the density-weighted displacement speed.

The current analysis indicated that the curvature and strain rate dependencies need to be accounted for in the modeling of the surface-averaged/filtered density-weighted displacement speed $\overline{\left(S_d^*\right)}_s$ in such a manner that the change in correlation strengths with strain rate and curvature based on local conditions of HOI and wall boundary conditions can be accurately captured in RANS/LES modeling.

It was reported by Kai et al. (2022) that the qualitative behaviour of mean values of displacement speed and its components across the flame front does not change due to the variation of Re_τ in FWI within turbulent boundary layers but further analyses based on detailed chemistry at higher values of Re_τ will be necessary for quantitative predictions and deeper understanding despite previous analyses by Keil et al. (2021a, 2021b) and Lai, Klein, and Chakraborty (2018, 2022) demonstrated that the displacement speed and the global features of FWI, respectively, can be captured, at least in the qualitative sense, with the help of single-step chemistry for methane-air flames. However, further analyses based on detailed chemistry at higher values of Re_τ will be necessary for quantitative predictions and deeper understanding.

Disclosure statement

No potential conflict of interest was reported by the author(s).

Funding

The authors are grateful for the financial and computational support from the Engineering and Physical Sciences Research Council [Grant: EP/V003534/1 and EP/R029369/1], ARCHER2 pioneer project (e691), CIRRUS, and ROCKET HPC facility.

References

Ahmed, U., D. Apsley, T. Stallard, P. Stansby, and I. Afgan. 2021. Turbulent length scales and budgets of reynolds stress-transport for open-channel flows; friction reynolds numbers Re_τ=150, 400 and 1020. *J. Hydraul. Res.* 59 (1):36–50. doi:10.1080/00221686.2020.1729265.

Ahmed, U., N. Chakraborty, and M. Klein. 2021a. Assessment of Bray Moss Libby formulation for premixed flame-wall interaction within turbulent boundary layers: Influence of flow configuration. *Combust. Flame* 233:111575. doi:10.1016/j.combustflame.2021.111575.

Ahmed, U., N. Chakraborty, and M. Klein. 2021b. Influence of thermal wall boundary condition on scalar statistics during flame-wall interaction of premixed combustion in turbulent boundary layers. *Int. J. Heat Fluid Flow* 82:108881. doi:10.1016/j.ijheatfluidflow.2021.108881.

Ahmed, U., N. Chakraborty, and M. Klein. 2021c. Scalar gradient and strain rate statistics in oblique premixed flame–wall interaction within turbulent channel flows. *Flow, Turb. and Combust.* 106 (2):701–32. doi:10.1007/s10494-020-00169-3.

Ahmed, U., N. Chakraborty, and M. Klein. 2023. Infuence of flow confguration and thermal wall boundary conditions on turbulence during premixed Flame-wall interaction within low reynolds number boundary layers, flow, Turb. *Flow, Turb. and Combust.* 111 (3):825–66. doi:10.1007/s10494-023-00437-y.

Ahmed, U., N. A. K. Doan, J. Lai, M. Klein, N. Chakraborty, and N. Swaminathan. 2018. Multiscale analysis of head-on quenching premixed turbulent flames. *Phys. Fluids* 30 (10):105102. doi:10.1063/1.5047061.

Ahmed, U., A. L. Pillai, N. Chakraborty, and R. Kurose. 2020. Surface density function evolution and the influence of strain rates during turbulent boundary layer flashback of hydrogen-rich premixed combustion. *Phys. Fluids* 32 (5):055112. doi:10.1063/5.0004850.

Alshaalan, T. M., and C. J. Rutland. 1998. Turbulence, scalar transport, and reaction rates in flame-wall interaction. *Proc. Combust. Inst.* 27 (1):793–99. doi:10.1016/S0082-0784(98)80474-8.

Alshaalan, T. M., and C. J. Rutland. 2002. Wall heat flux in turbulent premixed reacting flow. *Combust. Sci. Technol* 174 (1):135–65. doi:10.1080/713712913.

Boger, M., D. Veynante, H. Boughanem, and A. Trouvé. 1998. Direct numerical simulation analysis of flame surface density concept for large eddy simulation of turbulent premixed combustion. *Proc. Combust. Inst.* 27 (1):917–25. doi:10.1016/S0082-0784(98)80489-X.

Bruneaux, G., K. Akselvol, T. Poinsot, and J. H. Ferziger. 1996. Flame-wall interaction simulation in a turbulent channel flow. *Combust. Flame* 107 (1–2):27–36. doi:10.1016/0010-2180(95)00263-4.

Chakraborty, N. 2007. Comparison of displacement speed statistics of turbulent premixed flames in the regimes representing combustion in corrugated flamelets and thin reaction zones. *Phys. Fluids* 19 (10):105109. doi:10.1063/1.2784947.

Chakraborty, N., and R. S. Cant. 2005. Influence of Lewis number on curvature effects in turbulent premixed flame propagation in the thin reaction zones regime. *Phys. Fluids* 17 (10):105105. doi:10.1063/1.2084231.

Chakraborty, N., and R. S. Cant. 2006. Influence of lewis number on strain rate effects in turbulent premixed flame propagation in the thin reaction zones regime. *Int. J. Heat Mass Trans* 49 (13–14):2158–72. doi:10.1016/j.ijheatmasstransfer.2005.11.025.

Chakraborty, N., and R. S. Cant. 2007. A priori analysis of the curvature and propagation terms of the flame surface density transport equation for large eddy simulation. *Phys. Fluids* 19 (10):105101. doi:10.1063/1.2772326.

Chakraborty, N., and R. S. Cant. 2009. Direct numerical simulation analysis of the flame surface density transport equation in the context of large eddy simulation. *Proc. Combust. Inst.* 32 (1):1445–53. doi:10.1016/j.proci.2008.06.028.

Chakraborty, N., and S. Cant. 2004. Unsteady effects of strain rate and curvature on turbulent premixed flames in an inflow–outflow configuration. *Combust. Flame* 137 (1–2):129–47. doi:10.1016/j.combustflame.2004.01.007.

Chakraborty, N., G. Hartung, M. Katragadda, and C. F. Kaminski. 2011. A numerical comparison of 2D and 3D density-weighted displacement speed statistics and implications for laser based measurements of flame displacement speed. *Combust. Flame* 158 (7):1372–90. doi:10.1016/j.combustflame.2010.11.014.

Chakraborty, N., E. R. Hawkes, J. H. Chen, and R. S. Cant. 2008. The effects of strain rate and curvature on surface density function transport in turbulent premixed methane–air and hydrogen–air flames: A comparative study. *Combust. Flame* 154 (1–2):259–80. doi:10.1016/j.combustflame.2008.03.015.

Chakraborty, N., A. Herbert, U. Ahmed, H. G. Im, and M. Klein. 2022. Assessment of extrapolation relations of displacement speed for detailed chemistry direct numerical simulation database of statistically planar turbulent premixed flames. *Flow Turb. Combust* 108:489–507.

Chakraborty, N., and M. Klein. 2008. Influence of Lewis number on the surface density function transport in the thin reaction zones regime for turbulent premixed flames. *Phys. Fluids* 20 (6):065102. doi:10.1063/1.2919129.

Chakraborty, N., M. Klein, and R. S. Cant. 2007. Stretch rate effects on displacement speed in turbulent premixed flame kernels in the thin reaction zones regime. *Proc. Combust. Inst.* 31 (1):1385–92. doi:10.1016/j.proci.2006.07.184.

Chakraborty, N., M. Klein, and R. S. Cant. 2011. Effects of turbulent reynolds number on the displacement speed statistics in the thin reaction zones regime turbulent premixed combustion. *J. Combust* 473679 (1). doi:10.1155/2011/473679.

Chen, J. H., and H. G. Im. 1998. Correlation of flame speed with stretch in turbulent premixed Methane/Air flames. *Proc. Combust. Inst.* 27 (1):819–26. doi:10.1016/S0082-0784(98)80477-3.

Chen, J. H., and H. G. Im. 2000. Stretch effects on the burning velocity of turbulent premixed Hydrogen/Air flames. *Proc. Combust. Inst.* 28 (1):211–18. doi:10.1016/S0082-0784(00)80213-1.

Echekki, T., and J. H. Chen. 1996. Unsteady strain rate and curvature effects in turbulent premixed methane-air flames . *Proc. Combust. Flame* 106 (1–2):184–202. doi:10.1016/0010-2180(96)00011-9.

Echekki, T., and J. H. Chen. 1999. Analysis of the contribution of curvature to premixed flame propagation. *Combust. Flame* 118 (1–2):303–11. doi:10.1016/S0010-2180(99)00006-1.

Ghai, S. K., U. Ahmed, M. Klein, and N. Chakraborty. 2022. Energy integral equation for premixed flame-wall interaction in turbulent boundary layers and its application to turbulent burning velocity and wall flux evaluations. *Int. J. Heat & Mass Trans* 196:123230. doi:10.1016/j.ijheatmasstransfer.2022.123230.

Ghai, S. K., N. Chakraborty, U. Ahmed, and M. Klein. 2022. Enstrophy evolution during head-on wall interaction of premixed flames within turbulent boundary layers. *Phys. Fluids* 34 (7):075124. doi:10.1063/5.0098047.

Gran, I. R., T. Echekki, and J. H. Chen. 1996. Negative flame speed in an unsteady 2-D premixed flame: A computational study. *Proc. Combust. Inst.* 26 (1):211–18. doi:10.1016/S0082-0784(96)80232-3.

Gruber, A., J. H. Chen, D. Valiev, and C. K. Law. 2012. Direct numerical simulation of premixed flame boundary layer flashback in turbulent channel flow. *J. Fluid Mech* 709:516–42. doi:10.1017/jfm.2012.345.

Gruber, A., R. Sankaran, E. R. Hawkes, and J. H. Chen. 2010. Turbulent flame–wall interaction: A direct numerical simulation study. *J. Fluid Mech* 658:5–32. doi:10.1017/S0022112010001278.

Han, I., and K. H. Huh. 2008. Roles of displacement speed on evolution of flame surface density for different turbulent intensities and Lewis numbers for turbulent premixed combustion. *Combust. Flame* 152 (1–2):194–205. doi:10.1016/j.combustflame.2007.10.003.

Hawkes, E. R., and R. S. Cant. 2001. Implications of a flame surface density approach to large Eddy simulation of turbulent premixed combustion. *Combust. Flame* 126 (3):1617–29. doi:10.1016/S0010-2180(01)00273-5.

Haworth, D. C., and T. J. Poinsot. 1992. Numerical simulations of Lewis number effects in turbulent premixed flames. *J. Fluid Mech* 244 (–1):405–36. doi:10.1017/S0022112092003124.

Herbert, A., U. Ahmed, N. Chakraborty, and M. Klein. 2020. Applicability of extrapolation relations for curvature and stretch rate dependences of displacement speed for statistically planar turbulent premixed flames. *Combust. Theor. Modell* 24 (6):1021–38. doi:10.1080/13647830.2020.1802066.

Huang, W. M., S. R. Vosen, and R. Greif. 1988. Heat transfer during laminar flame quenching: Effect of fuels. *Proc. Combust. Inst.* 21 (1):1853–60. doi:10.1016/S0082-0784(88)80420-X.

Jarosinski, J. 1986. A survey of recent studies on flame extinction. *Prog. Ener. Combust. Sci* 12 (2):81–116. doi:10.1016/0360-1285(86)90014-6.

Jenkins, K. W. and R. S. Cant. 1999. Direct numerical simulation of turbulent flame kernels, recent advances in DNS and LES. *Fluid Mech. And Its Appl.* 54:191–202.

Kai, R., A. L. Pillai, U. Ahmed, N. Chakraborty, and R. Kurose. 2022. Analysis of the evolution of the surface density function during premixed V-Shaped flame–wall interaction in a turbulent channel flow at $Re_{\tau} = 395$. *Combust. Sci. Technol* 1–27. doi:10.1080/00102202.2022.2150971.

Keil, F. B., M. Amzehnhoff, U. Ahmed, N. Chakraborty, and M. Klein. 2021a. Comparison of flame propagation statistics extracted from direct numerical simulation based on simple and detailed chemistry—part 1: Fundamental flame turbulence interaction. *Energies* 14 (17):5548. doi:10.3390/en14175548.

Keil, F. B., M. Amzehnhoff, U. Ahmed, N. Chakraborty, and M. Klein. 2021b. Comparison of flame propagation statistics extracted from DNS based on simple and detailed chemistry part 2: Influence of choice of reaction progress variable. *Energies* 14 (18):5695. doi:10.3390/en14185695.

Kitano, T., T. Tsuji, R. Kurose, and S. Komori. 2015. Effect of pressure oscillations on flashback characteristics in a turbulent channel flow. *Energy. Fuels* 29 (10):6815–22. doi:10.1021/acs.energyfuels.5b01687.

Lai, J., U. Ahmed, M. Klein, and N. Chakraborty. 2022. A comparison between head-on quenching of stoichiometric methane-air and hydrogen-air premixed flames using direct numerical simulations. *Int. J. Heat Fluid Flow* 93:108896. doi:10.1016/j.ijheatfluidflow.2021.108896.

Lai, J. and N. Chakraborty. 2016. Effects of Lewis number on head on quenching of turbulent premixed flame: A direct numerical simulation analysis. *Flow Turb. Combust.* 96 (2):279–308. doi:10.1007/s10494-015-9629-x.

Lai, J., M. Klein, and N. Chakraborty. 2018. Direct numerical simulation of head-on quenching of statistically planar turbulent premixed methane-air flames using a detailed chemical mechanism. *Flow, Turb. Combust* 101:1073–91. doi:10.1007/s10494-018-9907-5.

Nivarti, G. V., and R. S. Cant. 2019. Stretch rate and displacement speed correlations for increasingly turbulent flames. *Flow, Turb. Combust.* 102 (4):957–71. doi:10.1007/s10494-018-9990-7.

Ozel-Erol, G., J. Hasslberger and N. Chakraborty 2022. Surface density function evolution in spherically expanding flames in globally stoichiometric droplet-laden mixtures. *Combust. Sci. Technol.* 194 (1):1–21.

Ozel-Erol, G., M. Klein, and N. Chakraborty. 2021. Lewis number effects on flame speed statistics in spherical turbulent premixed flames. *Flow, Turb. Combust* 106:1043–63. doi:10.1007/s10494-020-00173-7.

Peters, N. 2000. *Turbulent combustion, Cambridge monograph on mechanics*. Cambridge: Cambridge University Press.

Peters, N., P. Terhoeven, J. H. Chen, and T. Echekki. 1998. Statistics of flame displacement speeds from computations of 2-D unsteady methane-air flames. *Proc. Combust. Inst.* 27 (1):833–39. doi:10.1016/S0082-0784(98)80479-7.

Poinsot, T. J. A., and S. K. Lele 1992. Boundary conditions for direct simulations of compressible viscous flows. *J. Comput. Phys.* 101 (1):104–29.

Poinsot, T. J., D. C. Haworth, and G. Bruneaux 1993. Direct simulation and modeling of flame-wall interaction for premixed turbulent combustion. *Combust. and Flame* 95 (1–2):118–32.

Poinsot, T., and D. Veynante. 2005. *Theoretical and numerical combustion*. RT Edwards, Inc.

Renou, B., A. Boukhalfa, D. Peuchberty, and M. Trinité. 1998. Effects of stretch on the local structure of freely propagating premixed low-turbulent flames with various Lewis numbers. *Proc. Combust. Inst* 29 (1):841–47. doi:10.1016/S0082-0784(98)80480-3.

Sankaran, R., E. R. Hawkes, J. H. Chen, T. Lu, and C. K. Law. 2007. Structure of a spatially developing turbulent lean methane–air bunsen flame. *Proc. Combust. Inst.* 31 (1):1291–98. doi:10.1016/j.proci.2006.08.025.

Sellmann, J., J. W. Lai, A. M. Kempf, and N. Chakraborty. 2017. Flame surface density based modelling of head-on quenching of turbulent premixed flames. *Proc. Combust. Inst* 36 (2):1817–25. doi:10.1016/j.proci.2016.07.114.

Trouvé, A., and T. Poinsot. 1994. The evolution equation for the flame surface density in turbulent premixed combustion. *J. Fluid Mech* 278:1–31. doi:10.1017/S0022112094003599.

Vosen, S. R., R. Greif, and C. K. Westbrook. 1985. Unsteady heat transfer during laminar flame quenching. *Proc. Combust. Inst.* 20 (1):75–83. doi:10.1016/S0082-0784(85)80490-2.

Wray, A. A. 1990. Minimal storage time advancement schemes for spectral methods, unpublished report. NASA Ames Research Center, (CA).